European Journal of Medicinal Chemistry 214 (2021) 113256

Contents lists available at ScienceDirect

European Journal of Medicinal Chemistry

journal homepage: http://www.elsevier.com/locate/ejmech

Novel diaryl-2*H*-azirines: Antitumor hybrids for dual-targeting tubulin and DNA

Shibo Lin [a, 1], Yuru Liang [a, 1], Jiayi Cheng [a], Feng Pan [a], Yang Wang [a, b, *]

[a] School of Pharmacy, Fudan University, Shanghai, 201203, China
[b] Shanghai Key Laboratory for Molecular Engineering of Chiral Drugs, Shanghai Jiao Tong University, Shanghai, 200240, China

ARTICLE INFO

Article history:
Received 16 November 2020
Received in revised form
28 January 2021
Accepted 30 January 2021
Available online 3 February 2021

Keywords:
2,3-Diaryl-2*H*-azirine
Tubulin polymerization
DNA damage
Antitumor

ABSTRACT

Multiple-target drugs may achieve better therapeutic effect *via* different pathways than single-target ones, especially for complex diseases. Tubulin and DNA are well-characterized molecular targets for anti-cancer drug development. A novel class of diaryl substituted 2*H*-azirines were designed based on combination of pharmacophores from Combretastatin A-4 (CA-4) and aziridine-type alkylating agents, which are known tubulin polymerization inhibitor and DNA damaging agents, respectively. The antitumor activities of these compounds were evaluated *in vitro* and **6h** showed the most potent activities against four cancer cell lines with IC_{50} values ranging from 0.16 to 1.40 μM. Further mechanistic studies revealed that **6h** worked as a bifunctional agent targeting both tubulin and DNA. In the nude mice xenograft model, **6h** significantly inhibited the tumor growth with low toxicity, demonstrating the promising potential for further developing novel cancer therapy with a unique mechanism.

1. Introduction

Microtubules play a critical role in various cellular processes (e.g., formation of the mitotic spindle, intracellular transport, cell division, cell signaling and migration), and thus have generally been considered as an excellent target for development of antitumor agents [1,2]. Antimitotic agents are known to inhibit microtubule function by the dynamic balance of tubulin stabilization or destabilization, leading to mitotic arrest [3,4]. Combretastatin A-4 (CA-4, Fig. 1), a *cis*-stilbene-type natural compound isolated from the African willow tree *Combretum caffrum*, is a typical molecule that can bound tightly to the colchicine binding site of tubulin, leading to closed vessels and dead cells in neoplastic tissues. CA-4 has demonstrated strong cytotoxicity against many different types of neoplastic cells, including some multidrug-resistant ones [5,6]. The structure-activity relationship (SAR) of CA-4 and its derivatives revealed that the presence of a 3,4,5-trimethoxyphenyl as A-ring and the *cis*-form of the double bond are crucial for its potent antitumor activity [7,8]. Unfortunately, stability studies revealed that CA-4 is highly susceptible to *cis*/*trans* isomerization under physiological conditions, and its *trans* isomer is inactive against tumor cell proliferation [9]. A number of efforts have been devoted to resolve this problem, including the synthesis and evaluation of various CA-4 analogues whose pharmacophores are spatially confined by more rigid cores, typically *via* the substitution of the olefinic bond in CA-4 with heterocyclic moieties, such as β-lactam [10,11], hydantoin [12], thiazole [13], furan [14], imidazo[4,5-c]pyridin-2-one [15], pyrazole [16], etc, to maintain a suitable spatial orientation of two aromatic rings to achieve optimal bioactivity.

On the other hand, the DNA alkylating agents have also been widely applied clinically in cancer chemotherapy for many years [17]. One type of the earliest and perhaps most commonly used DNA cross-linking agents are derivatives of nitrogen mustard [18–20], in which the *N*,*N*-bis(2-chloroethyl)-amino pharmacophore can act as reactive electrophiles through the intramolecular transformation into aziridine ring [20]. As shown in Fig. 1, a similar pharmacophore also occurs in some clinical drugs, such as Thiotepa and Mitomycin C (MCC). Over the last several decades, they have generally been applied as constituents of cancer drug combinations against a number of cancers, including gastric, colorectal, breast, ovarian, bladder and non-small cell lung carcinoma [21,22].

* Corresponding author. School of Pharmacy, Fudan University, Shanghai, 201203, China.
E-mail address: wangyang@shmu.edu.cn (Y. Wang).
[1] contributed equally to this work.

https://doi.org/10.1016/j.ejmech.2021.113256
0223-5234/

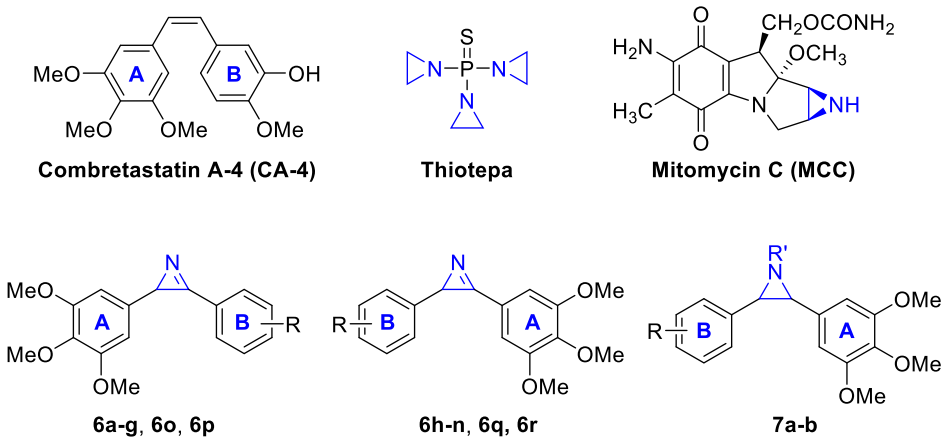

Fig. 1. Representative antitumor agents CA-4, Thiotepa and MCC, targeting tubulin and DNA, respectively, and the designed 2*H*-azirine and aziridine skeletal structures **6** and **7**.

MCC undergoes intracellular activation by interaction with cytochrome P450 reductase [23] or other 1- or 2-electron reductases [24], and the subsequent leaving of methoxy group generates MCC-leucoaziridinomitosene, which consequently incurs DNA alkylation under acidic condition [25]. In addition, the MCC-DNA monoadduct located within the DNA minor groove causes steric hindrance to further enzymatic reduction of the quinone ring. All these factors facilitate carbamate departure during subsequent DNA attachment and tend to produce MCC-DNA interstrand crosslinks (ICLs, Fig. 2) [26]. Moreover, researches showed that aziridine-bearing antitumor agents including thiotepa can generate covalent adducts with DNA double-helix strands *via* the alkylation of the N7 atom of guanine [27,28], resulting in the obstruction on DNA replication and transcription, and causing cell death.

Recent studies have indicated that DNA damaging agents, mainly platinum drugs, could enhance the apoptosis-inducing activity of tubulin inhibitors (Fig. 3) [29,30]. Compounds targeting both tubulin and DNA can in principle merge the two distinct anticancer pharmocophores into the structure of one agent, and thus may create potential synergy by itself. The dual tubulin polymerization inhibition and DNA damage functions might lead to an improvement in targeting and therapeutic efficacy, and this may represent an avenue towards the development of new anti-cancer agents [31–35].

In an effort to search for more effective compounds that target tubulin and DNA synergistically, we designed and investigated a new series of diaryl-2*H*-azirine derivatives based on the combination strategy for multitarget drug (Fig. 1). Among these compounds, compound **6h** exhibited satisfactory antineoplastic activity against several different cell lines. Further mechanism studies and *in vivo* activities demonstrated the promising potential of **6h** as a novel dual-targeting anticancer agent.

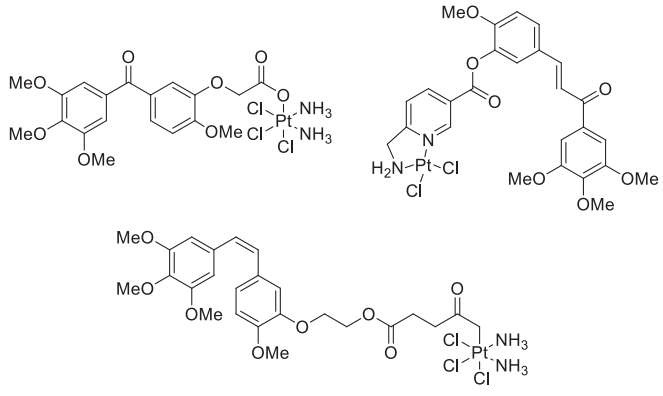

Fig. 3. The dual-target compounds acting on microtubules and DNA.

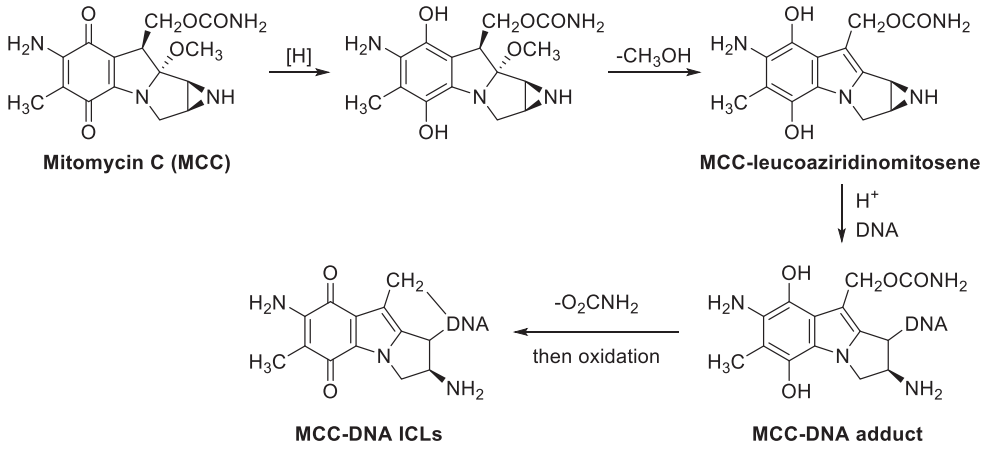

Fig. 2. Mechanism for MCC activation that induces DNA ICLs.

2. Results and discussion

2.1. Chemistry

The target compounds were synthesized by following the general procedures as outlined in Scheme 1. The reactions of commercially available aryl acetonitriles (**1a**-**r**) and arylboronic acids (**2a**-**r**) proceeded smoothly under Pd(II) catalysis [36], giving a variety of aryl alkyl ketones (**3a**-**r**) in good to excellent yields (75−87%). Condensation of these ketones (**3a**-**r**) with $NH_2OH·HCl$/K_2CO_3 gave corresponding ketoximes (**4a**-**r**), respectively. Subsequent esterification with acetic anhydride afforded the corresponding ketoxime acetates (**5a**-**r**), which were then cyclized by treatment with cesium carbonate [37] into 2*H*-azirines (**6a**-**r**) in good yields (67−81%). Reduction of **6h** with sodium borohydride in tetrahydrofuran produced 2-(3-fluoro-4-methoxyphenyl)-3-(3,4,5-trimethoxyphenyl)-aziridine (**7a**) in excellent yield (91%), and *N*-methylation of **7a** with methyl iodide gave **7b** in 81% yield. The relative configuration of **7a** was predicted to be *cis*-isomers, based on Feng group's work that the chiral diaryl-2*H*-azirines (93% *ee*) could be converted into corresponding *cis*-aziridines (93% *ee*) in presence of $NaBH_4$ with excellent diastereo- and enantioselectivity [38].

2.2. Anti-proliferation activities against four human cancer cell lines in vitro

The newly synthesized 2,3-diaryl-2*H*-azirines **6a**-**r** and aziridines **7a-b** were evaluated for anti-proliferative activities *in vitro* against A2780, HCT-116, A549 and HeLa human cancer cell lines, respectively, using CA-4 and Mitomycin C (MMC) as the reference compounds.

As shown in Table 1, most target compounds **6** and **7** exhibited moderate to excellent cytotoxicity against these tumor cells, especially on A2780. Among them, 2,3-diaryl-2*H*-azirines (**6a**, **6b**, **6e**, **6h** and **6m**) showed good activities with IC_{50} values in the range of 0.16−1.54 μM, while the aziridines **7a** and **7b** demonstrated a decrease in the antiproliferative activity (IC_{50} = 1.09−8.74 μM) compared with that of **6h** (IC_{50} = 0.16−1.40 μM). These results suggested that the rigid 2*H*-azirine core is likely to be more appropriate for fixing the orientation of two aryl substituents, so that the molecule can better bind to the colchicine site of β-tubulin. The exchange of A and B aromatic rings on the 2*H*-azirines exhibited few influence on the antiproliferative activity (**6a** and **6h**, **6b** and **6i**). In addition, it was found that compounds with 4-methoxy (**6a-b**, **6h-i** and **6g**), 4-methyl (**6f** and **6m**) or 4-methylthio (**6n**) substituents on the B ring exhibit enhanced potency compared to those of 4-ethoxy compounds (**6e** and **6l**), which implied that bulkier groups will compromise the activity to a

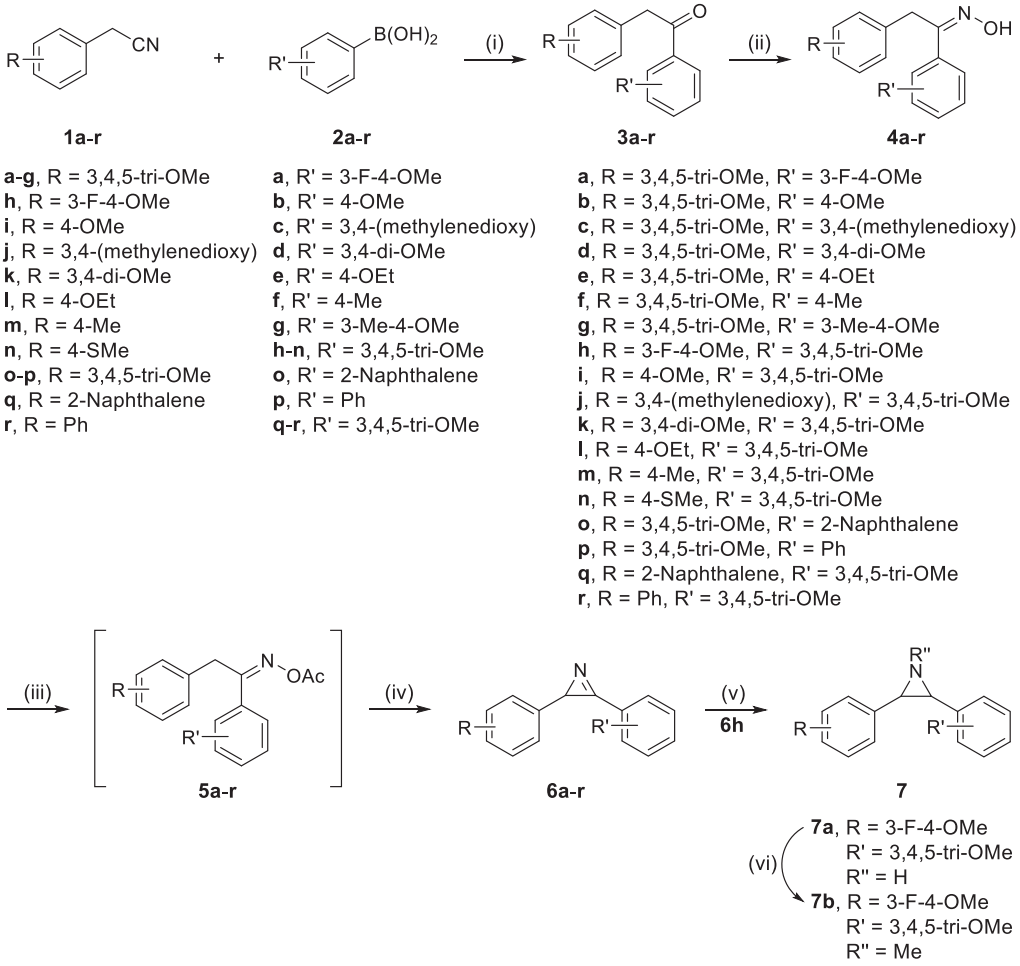

Scheme 1. Synthesis of 2*H*-azirines (**6a**-**r**) and aziridines (**7a**-**b**). Reagents and conditions: (i) $Pd(OAc)_2$, 2,2′-Bipyridine, TFA, KF, THF/H_2O, 80 °C, 2 h; (ii) $NH_2OH·HCl$, K_2CO_3, MeOH, 50 °C, 5 h; (iii) Ac_2O, TEA, DCM, r.t., 30 min; (iv) K_2CO_3, DMF, 80 °C, 1 h; (v) $NaBH_4$, THF, r.t., 2 h; (vi) MeI, r.t., 3 h.

Table 1
Antiproliferative activities of compounds **6** and **7** on different cell lines.

Compound	IC_{50} (μM)[a]			
	A2780[b]	HCT-116[c]	HeLa[d]	A549[e]
6a	0.19	0.32	0.73	0.63
6b	0.44	0.76	1.54	1.12
6c	1.54	0.97	1.52	9.16
6d	2.66	12.40	12.66	17.57
6e	0.58	0.50	1.14	0.76
6f	0.17	0.79	2.07	2.30
6g	0.58	3.59	2.65	6.33
6h	0.16	0.63	1.07	1.40
6i	0.33	1.10	1.97	1.49
6j	1.74	1.89	2.02	2.21
6k	2.92	8.72	4.17	11.05
6l	0.78	1.10	1.96	3.61
6m	0.24	0.58	0.78	1.40
6n	0.40	1.51	2.19	4.16
6o	3.479	2.218	4.498	4.227
6p	0.927	2.058	1.933	1.820
6q	8.333	4.103	11.82	7.031
6r	3.479	2.218	4.498	4.227
7a	1.90	1.84	1.09	1.20
7b	4.68	5.44	4.39	8.74
CA-4	0.004	0.004	0.004	0.004
MMC	0.18	0.56	0.20	0.63

[a] The anti-proliferation activities of individual compound to tumor cells were determined by the MTT assay. The data are the mean of triplicate determinations.
[b] A2780 is a human ovarian cancer cell line.
[c] HCT-116 is a human colon carcinoma cell line.
[d] HeLa is a human cervical carcinoma cell line.
[e] A549 is a human lung adenocarcinoma cell line.

certain extent presumably due to steric factors. Compared with 3-methoxy (**6d**, **6k**) or 3,4-(methylenedioxy) (**6c**, **6j**) analogues, the potency could be promoted for compounds with no substituent (**6b**, **6e-f**, **6i**, **6l-n**) or fluorine (**6a**, **6h**) existing at the 3-position of B ring.

Among the target compounds synthesized, **6h** was selected to further investigate its pharmacological properties and action mechanism.

2.3. Inhibition of tubulin polymerization

Inhibitory effects of tubulin polymerization by the representative compound **6h** was tested using isolated pig brain tubulin. As shown in Fig. 4A and Table 2, tubulin polymerization was suppressed dependent on the concentration of **6h** with an IC_{50} value of 3.3 μM, which exhibited better inhibitory activity than the positive control colchicine.

Furthermore, cellular immunofluorescence assay was performed to confirm the inhibitory effects of **6h** on microtubule organization. As shown in Fig. 4B, the microtubule networks (green) possessed the characteristic of a normal arrangement with the cell nucleus were surrounded by slim and fibrous microtubules, indicating tubulin assembly was not affected. However, when HeLa cells were treated with **6h**, the microtubule networks were found to be disorganized and shrunk to the cell border (as the red arrows indicated), indicating that the presence of **6h** effectively induced the disruption of the microtubule networks, and eventually resulted in cell apoptosis.

2.4. Alkaline single cell gel electrophoresis (comet) assay and the detection of DNA damage inducing factor

The comet assay is a commonly used, sensitive method to investigate DNA damage in individual cells [39]. To test whether the 2*H*-azirine-based **6h** could induce DNA damage, Jurkat cells were treated with **6h** at gradient concentrations, and afterwards alkaline comet assay was used to evaluate the DNA damage. As shown in Fig. 5A–D, significant DNA lesions were observed for the sample treated with the positive control drug MMC at the concentration of 200 nM. Noteworthily, DNA damaged by **6h** emerged comparable tail moments at the same concentration as that of MCC, and the extent of DNA lesion was dose-dependent. In addition, DNA damage related proteins was characterized by proapoptotic Bax protein and growth arrest GADD45α that play an essential role in cell cycle checkpoint after exposure to certain DNA lesions such as alkylating agents and UV irradiation [40]. As shown in Fig. 5E, the compound **6h** significantly up-regulate expression of proapoptotic protein Bax and GADD45α in a dose-dependent manner. These observations suggested that **6h** could induce DNA damage.

2.5. Induction of cellular apoptosis

To assess whether compound **6h** could induce apoptosis of cell, the **6h-**treated HeLa cells were stained with Annexin V-FITC and propidium iodide (PI), which could be used to distinguish among live cells (annexin-V^-/PI^-), early apoptotic cells (annexin-V^+/PI^-), late apoptotic cells (annexin-V^+/PI^+), and necrotic cells (annexin-V^-/PI^+). The flow cytometric data (Fig. 6A and B) demonstrated a potent activity of **6h** on the apoptosis induction.

In addition, we examined the expression levels of apoptosis associated proteins *via* immunoblotting analysis. As indicated in Fig. 6C, proapoptotic protein p53 was up-regulated by **6h** in a dose-dependent manner. Additionally, **6h** was found to dose-dependently promote cleavage of poly(ADP-ribose) polymerase-1 (PARP-1), a marker of cells undergoing apoptosis. These results implied that the azirine analogues exhibited their antitumor activity through induction of cellular apoptosis.

2.6. Cell cycle analysis

To explore the influence of **6h** on cell cycle arrest, a cell cycle analysis was conducted by quantitiating the DNA content. The HeLa cells were treated with **6h** at various concentrations for 24 h, respectively, followed by being stained with propidium iodide, and the samples were analyzed by flow cytometry. As expected, cell cycle arrest was found to be induced by **6h** at G_2/M phase (Fig. 7A and B). In addition, the treatment with **6h** also up-regulated the expression of the phosphorylation of Histone H3, Cyclin B1 and BubR1, further supporting that **6h** could trigger cellular mitotic arrest in protein level (Fig. 7C).

2.7. Inhibition of colony formation

Further studies were performed to investigate the cytotoxic effects of **6h** by colony formation assays. As shown in Fig. 8, the colonies formed by HeLa were inhibited by exposure to **6h** in the dose dependent manner.

2.8. Anti-angiogenic effects in vitro

The tumor vascular disrupting activity of microtubule binding agents can significantly disturb the microtubule dynamics, which would in turn affect angiogenesis. The anti-angiogenic effect of **6h** was evaluated in a tube formation assay, based on the ability of human umbilical vein endothelial cells (HUVECs) to form cord-like and tubular networks on Matrigel, an extracellular matrix possessing fertile proangiogenic cytokines. As shown in Fig. 9, the HUVEC cells treated with only the DMSO control produced a complete network structure, while the introduction of **6h** into the system obviously altered the capillary-like structures in a dose-dependent manner. These results showed that **6h** effectively restrained the tube formation of HUVECs.

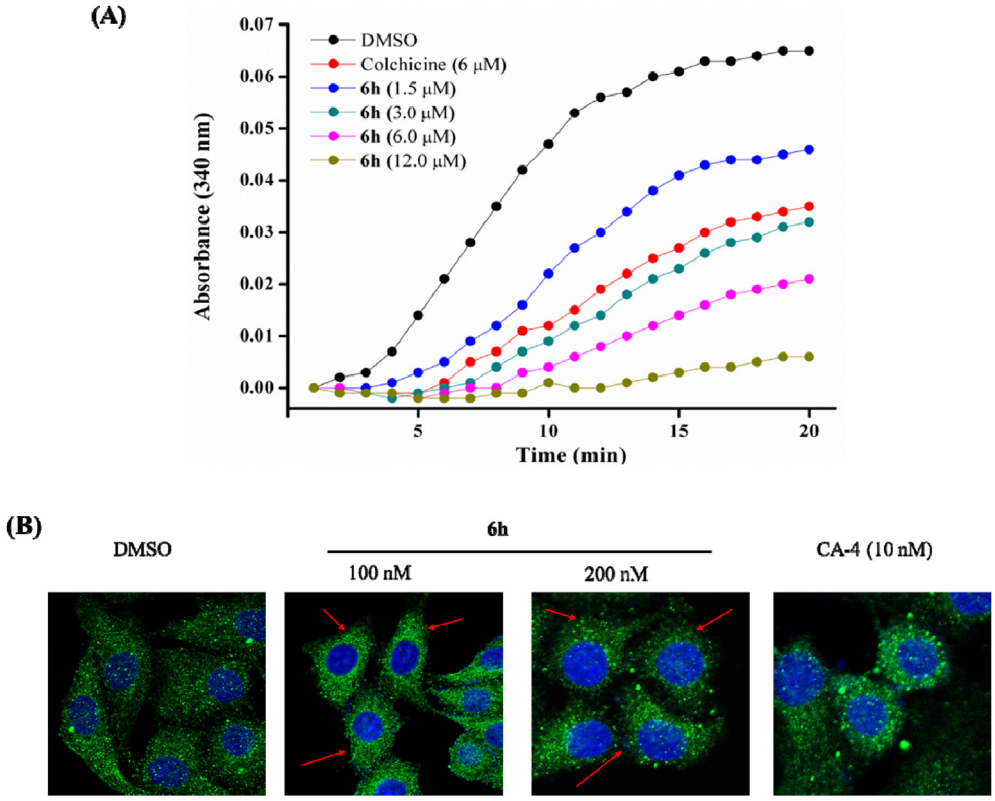

Fig. 4. (A) Effects of **6h** on tubulin polymerization *in vitro*. (B) Effects of **6h** on the organization of cellular microtubule networks.

Table 2
IC_{50} values of **6h** on inhibition of tubulin polymerization.

Compound	**6h**	Colchicine
IC_{50} (μM)	3.3	10.4

2.9. Anti-tumor activities in vivo

We established A2780 cells xenograft model to evaluate the anti-tumor activity of compound **6h**. When the tumor volume reached 100 mm^3, the nude mice were placed in four groups randomly (n = 10 for each group), control, Paclitaxel (PTX) and **6h** with two doses. As shown in Fig. 10A, in contrast to the fast tumor growth of the control group, treatment of **6h** dose-dependently inhibited tumor growth, and the efficacy of 50 mg/kg **6h** was found to be similar to that of PTX group. After the observation time period, the weight of stripped tumor was collected and the analysis results were shown in Fig. 10C and D, which demonstrated the potent activity of **6h**. Moreover, compared with the control group, **6h** caused no obvious weight loss (Fig. 10B), which implied that **6h** displayed no indications of toxicity or other adverse reactions in these mice, even at high dosage. These data strongly demonstrated that compound **6h** has potent anti-tumor efficacy with a reasonable therapeutic window *in vivo*.

2.10. Optical resolution and antitumor evaluation

In order to clarify the impact of stereochemistry on the activity, racemic **6h** was submitted to optical resolution by chiral HPLC, yielding enantiopure (−)-**6h** (100% *ee*) and (+)-**6h** (100% *ee*). As shown in Table 3, further antiproliferative evaluation indicated that there is no significant difference in the activities between (+)-**6h** and (−)-**6h**.

2.11. Absolute configuration

In order to confirm the absolute configuration of compound **6h**, (+)-**6h** was synthetically elaborated by borohydride reduction and sulfonylation, and the absolute configuration of the corresponding sulfonamide derivative **8** was determined as (2*R*, 3*S*) by X-ray single crystal diffraction, indicating that (+)-**6h** was (*R*)-configuration (Scheme 2).

3. Conclusion

In this research, a novel series of 2,3-diaryl-2*H*-azirines were designed and synthesized based on the combination principles, among which compound **6h** exhibited a remarkably potent anti-proliferative activity against four cancer cell lines. Further pharmacological studies demonstrated that **6h** could target both tubulin and DNA via tubulin polymerization assay and the comet assay, respectively. Moreover, **6h** could block cell cycle progression at the G_2/M phase, induce cell apoptosis, inhibit angiogenic activity, possess favorable metabolic stability, and significantly suppress xenografts tumor growth and show low toxicity. The anti-proliferative activity between enantiomers (*R*)-(+)-**6h** and (*S*)-(−)-**6h** demonstrated no significant difference. Consequently, such strategy by merging two different types of pharmacophores into one agent can provide an effective therapy.

4. Experimental section

4.1. General

Melting points were measured on an SGW X-4 apparatus which was uncorrected. ^1H and ^{13}C spectra were obtained by a Varian 400 MHz or a Bruker 600 MHz NMR spectrometer at 303 K, using

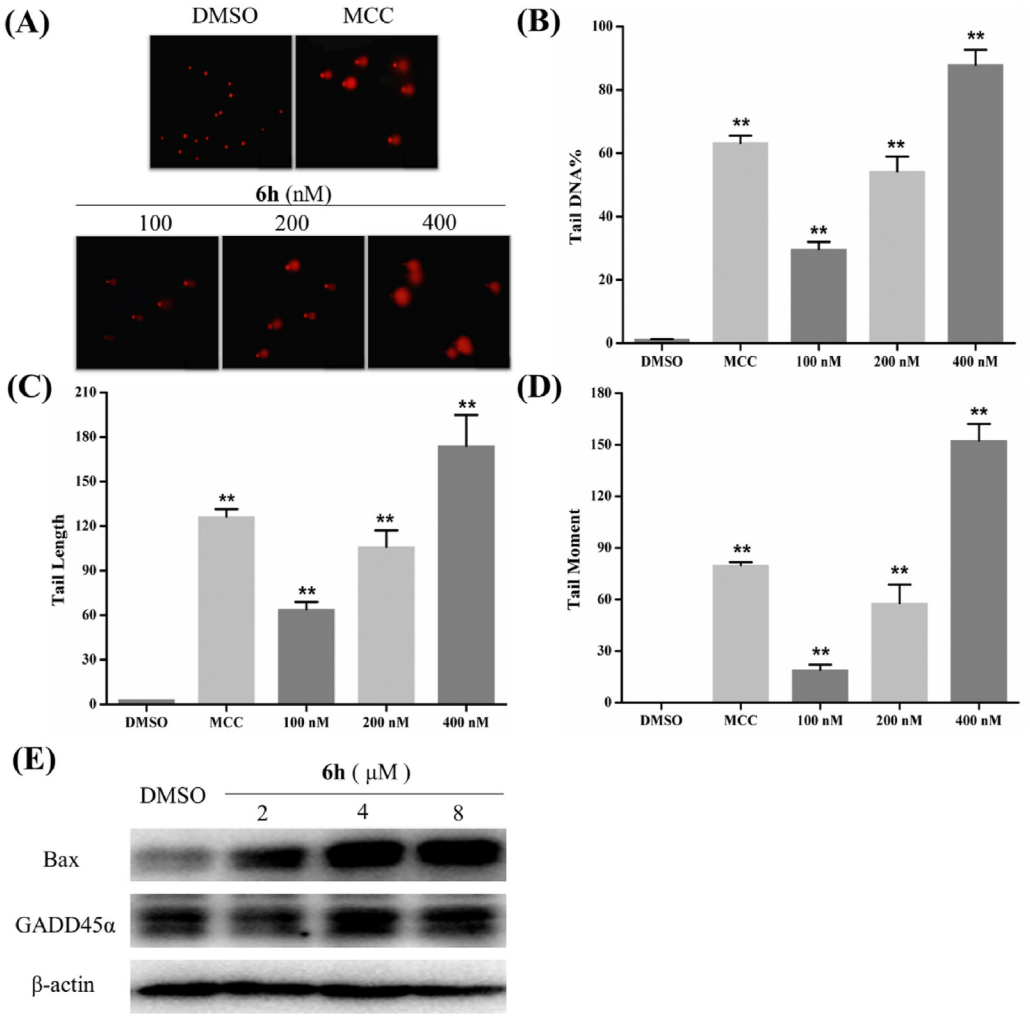

Fig. 5. The effect of **6h** on DNA damage response in Jurkat cells. Jurkat cells were treated with a DMSO solution **6h** (at the specified concentrations), MCC or DMSO for 48 h, respectively. Representative fluorescent images of Jurkat cells following the modified alkaline comet assay and EB staining (A). Throught Comet Assay Software Pect (CASP 1.2.3 beta 1), Tail DNA% (B), Tail length (C), Tail moment (D) were calculated, respectively. (E) Western blot analysis of DNA damage-related proteins.

$CDCl_3$ or DMSO-d_6 as the solvent with tetramethylsilane (TMS) as an internal standard at room temperature. High-resolution mass spectra were collected on an Agilent 6224 TOF LC/MS system. Commercially obtained reagents and solvents were used without further purification. Reactions were monitored by thin layer chromatography (TLC) by using silica gel (60, GF 254) coated glass slides and detected using UV light (254 nm). Flash chromatography was performed with standard silica gel 60 (200–300 mesh). The purity of all the compounds for bioactivity testing was confirmed to be $\geq$ 95% by HPLC detection.

4.2. General procedure for the synthesis of ketones (**3a**-**r**)

Under a nitrogen atmosphere, aryl acetonitrile **1** (3 mmol), arylboronic acids **2** (6 mmol), palladium acetate (5 mol %), 2,2′-Bipyridine (10 mol %), trifluoroacetic acid (30 mmol), potassium fluoride (6 mmol), tetrahydrofuran (20 mL), and water (10 mL) were successively added to a Schlenk reaction tube. The reaction mixture was stirred vigorously at 80 °C for 2 h. After the reaction mixture was cooled to room temperature, saturated sodium bicarbonate (30 mL) was added into the solution, and the mixture was extracted with ethyl acetate (10 mL) for 3 times. The combined organic layer was concentrated in vacuo. The residue was purified by flash column chromatography to afford desired product **3**.

4.2.1. 1-(3-fluoro-4-methoxyphenyl)-2-(3,4,5-trimethoxyphenyl) ethan-1-one (**3a**)

White solid. Yield 85%. Mp 106.5–109.3 °C. ^{1}H NMR (400 MHz, $CDCl_3$) δ 7.81 (d, J = 8.4 Hz, 1H), 7.76 (d, J = 11.9 Hz, 1H), 7.00 (t, J = 8.3 Hz, 1H), 6.46 (s, 2H), 4.16 (s, 2H), 3.96 (s, 3H), 3.84 (s, 6H), 3.83 (s, 3H). ^{13}C NMR (150 MHz, $CDCl_3$) δ 195.32, 153.37, 152.81, 152.05, 151.98, 151.16, 136.94, 130.03, 129.75, 129.72, 126.00, 125.98, 116.27, 116.14, 112.37, 106.35, 60.83, 56.30, 56.11, 45.47. ESI-HRMS (m/z): calcd for $C_{18}H_{19}FO_5Na$ (M + Na^+), 357.1108; found, 357.1119.

4.2.2. 1-(4-methoxyphenyl)-2-(3,4,5-trimethoxyphenyl)ethan-1-one (**3b**)

Light yellow solid. Yield 82%. Mp 84.9–87.5 °C. ^{1}H NMR (400 MHz, $CDCl_3$) δ 8.01 (d, J = 8.5 Hz, 2H), 6.94 (d, J = 8.4 Hz, 2H), 6.48 (s, 2H), 4.18 (s, 2H), 3.87 (s, 3H), 3.83 (s, 9H). ^{13}C NMR (150 MHz, $CDCl_3$) δ 196.20, 163.62, 153.29, 136.80, 130.92, 130.52, 129.57, 113.83, 106.40, 60.83, 56.09, 55.50, 45.46. ESI-HRMS (m/z): calcd for $C_{18}H_{20}O_5Na$ (M + Na^+), 339.1202; found, 339.1199.

4.2.3. 1-(benzo[d] [1,3]dioxol-5-yl)-2-(3,4,5-trimethoxyphenyl) ethan-1-one (**3c**)

White solid. Yield 76%. Mp 117.4–119.0 °C. ^{1}H NMR (400 MHz, $CDCl_3$) δ 7.64 (d, J = 8.1 Hz, 1H), 7.48 (s, 1H), 6.86 (d, J = 8.1 Hz, 1H), 6.46 (s, 2H), 6.05 (s, 2H), 4.15 (s, 2H), 3.84 (s, 6H), 3.83 (s, 3H). ^{13}C

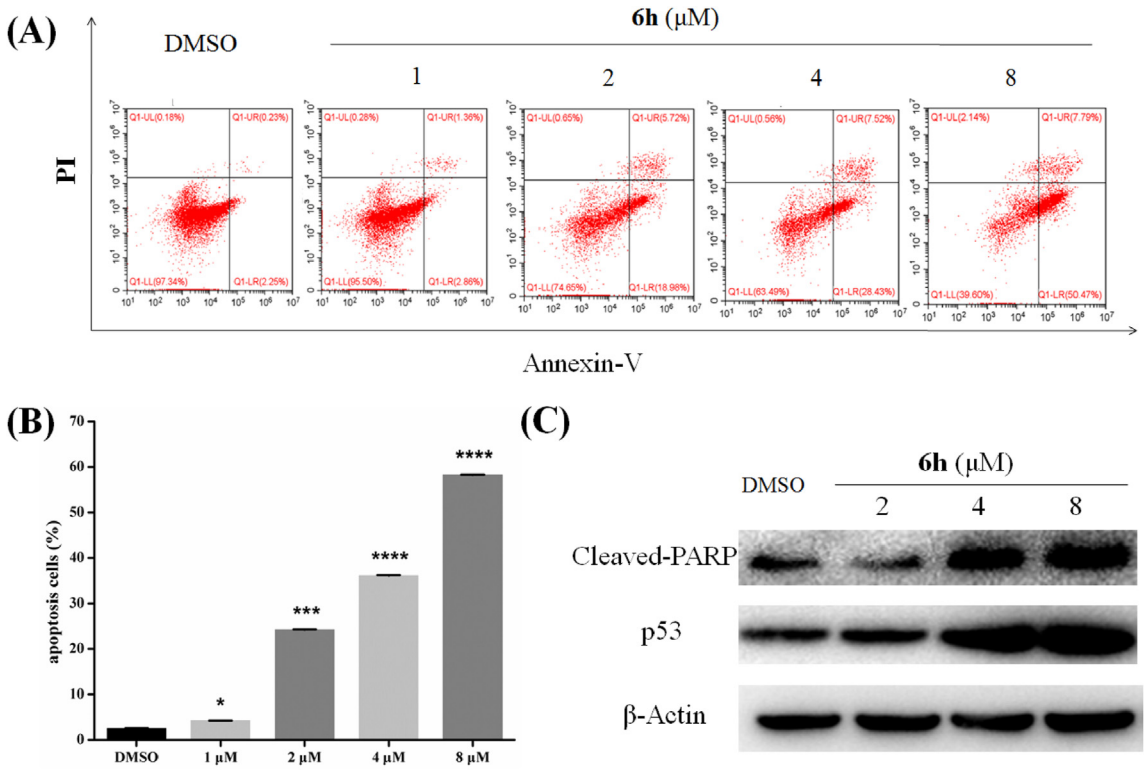

Fig. 6. (A) Flow cytometry profiles indicated that **6h** does-dependently promoted Hela cells apoptosis. (B) Statistic showed that **6h** caused apoptosis of Hela cells. (C) Western blot analysis of cell apoptosis-related proteins.

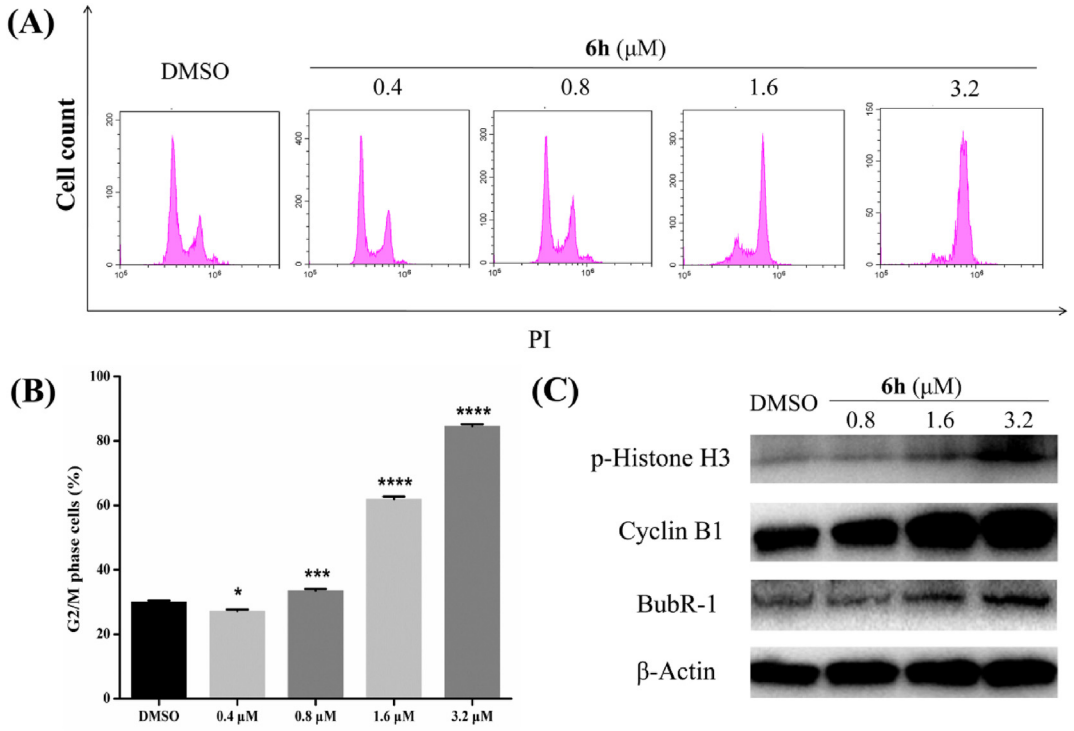

Fig. 7. Compound **6h** regulated HeLa cell cycle progression. (A) Compound **6h** could dose-dependently arrest cell cycle. (B) Statistic showed that **6h** induced G_2/M phase arrest in HeLa cells. (C) Cell cycle-related proteins were analyzed by western blot analysis.

NMR (151 MHz, $CDCl_3$) δ 195.71, 153.32, 151.94, 148.27, 136.85, 131.34, 130.34, 124.99, 108.34, 107.94, 106.35, 101.92, 60.84, 56.10, 45.54. ESI-HRMS (*m/z*): calcd for $C_{18}H_{18}O_6Na$ ($M + Na^+$), 353.0995; found, 353.0996.

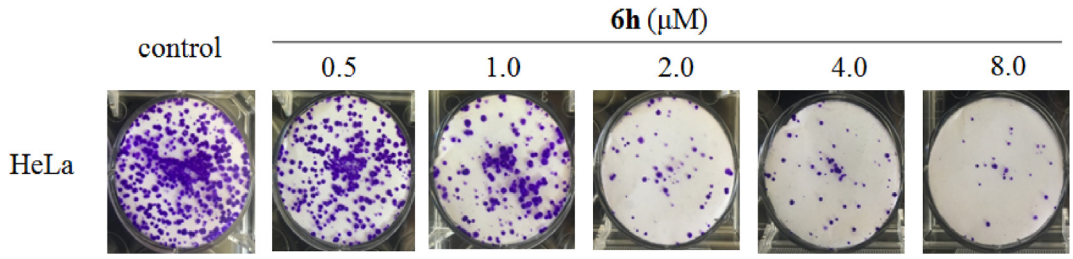

Fig. 8. Compound **6h** dose-dependently inhibited cell colony formation of HeLa cells.

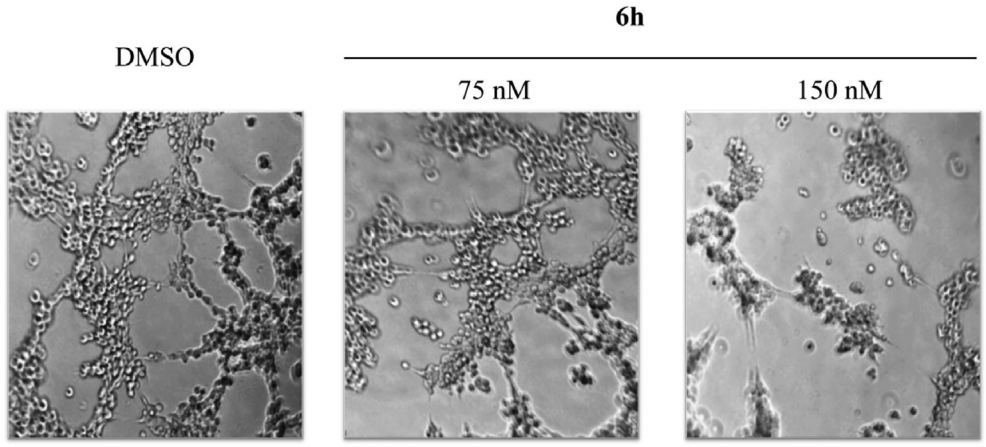

Fig. 9. Effects on the formation of a HUVEC capillary-like tubular network.

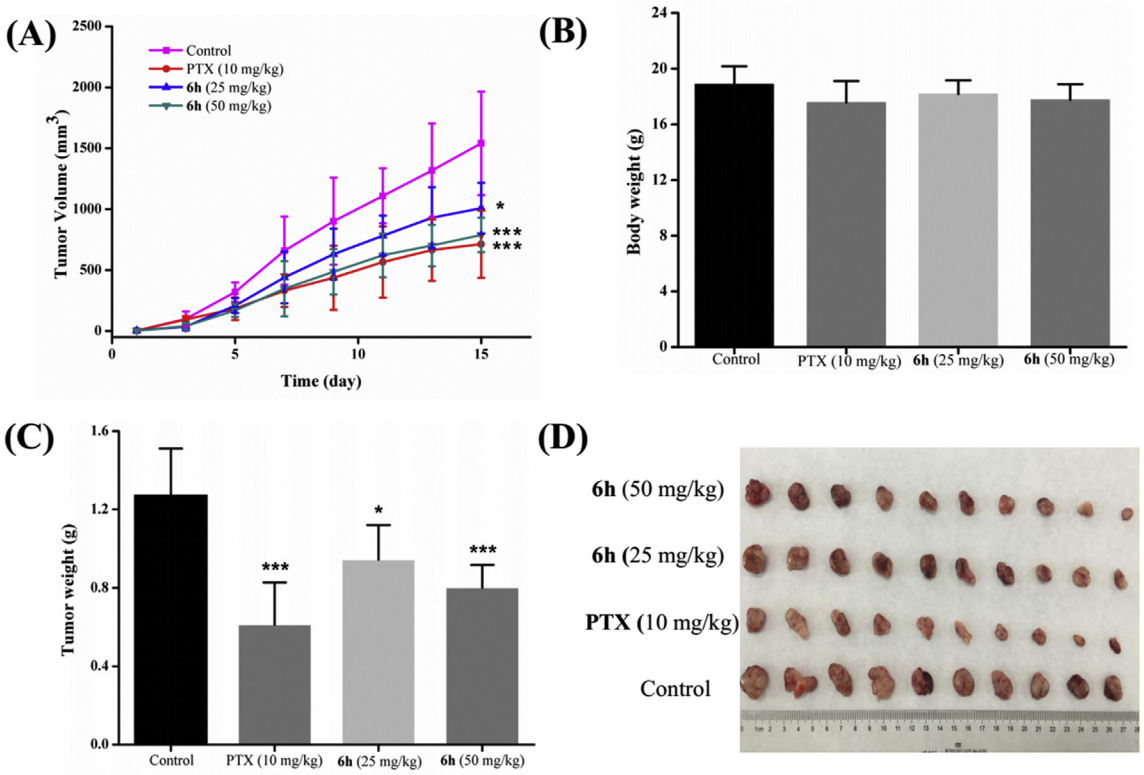

Fig. 10. Antitumor effect of **6h** on the A2780 xenograft models. At the end of observation, tumor volumes (A), body weights (B), tumor weights (C) and representative isolated tumors (D) were measured, respectively. Tumor volumes were gauged by vernier caliper every other day. Results represented the means ± SD. *$p < 0.05$, ***$p < 0.001$ *vs* untreated control.

Table 3
Enantiomers of **6h** and their antiproliferative activities.

Compound	[α]25 D	*ee*	IC_{50} (μM)			
			A2780	HCT-116	HeLa	A549
(+)-**6h**	+356.18	100%	0.12	0.57	0.89	1.18
(−)-**6h**	−355.87	100%	0.20	0.66	0.72	1.02
6h			0.16	0.63	0.87	1.19

*4.2.4. 1-(3,4-dimethoxyphenyl)-2-(3,4,5-trimethoxyphenyl)ethan-1-one (**3d**)*

Light yellow solid. Yield 79%. Mp 151.2–156.1 °C. ^{1}H NMR (400 MHz, CDCl $_3$) δ 7.68 (d, J = 8.3 Hz, 1H), 7.57 (s, 1H), 6.90 (d, J = 8.3 Hz, 1H), 6.49 (s, 2H), 4.19 (s, 2H), 3.95 (s, 3H), 3.93 (s, 3H), 3.84 (s, 6H), 3.83 (s, 3H). ^{13}C NMR (150 MHz, $CDCl_3$) δ 196.25, 153.44, 153.32, 149.11, 136.85, 130.58, 129.72, 123.44, 110.61, 110.00, 106.36, 60.84, 56.10, 55.97, 45.37. ESI-HRMS (*m/z*): calcd for $C_{19}H_{22}O_6Na$ ($M + Na^+$), 369.1308; found, 369.1302.

*4.2.5. 1-(4-ethoxyphenyl)-2-(3,4,5-trimethoxyphenyl)ethan-1-one (**3e**)*

Light yellow solid. Yield 87%. Mp 99.6–101.1 °C.^{1}H NMR (400 MHz, $CDCl_3$) δ 7.99 (d, J = 8.4 Hz, 2H), 6.93 (d, J = 8.4 Hz, 2H), 6.48 (s, 2H), 4.17 (s, 2H), 4.10 (q, J = 6.6 Hz, 2H), 3.83 (s, 6H), 3.82 (s, 3H), 1.44 (t, J = 6.8 Hz, 3H). ^{13}C NMR (150 MHz, $CDCl_3$) δ 196.18, 163.06, 153.28, 136.80, 130.92, 130.56, 129.38, 114.25, 106.41, 63.79, 60.83, 56.09, 45.42, 14.67. ESI-HRMS (*m/z*): calcd for $C_{19}H_{22}O_5Na$ ($M + Na^+$), 353.1359; found, 353.1355.

*4.2.6. 1-(p-tolyl)-2-(3,4,5-trimethoxyphenyl)ethan-1-one (**3f**)*

Red solid. Yield 84%. Mp 86.4–89.5 °C.^{1}H NMR (400 MHz, $CDCl_3$) δ 7.92 (d, J = 8.2 Hz, 2H), 7.27 (d, J = 8.2 Hz, 2H), 6.48 (s, 2H), 4.20 (s, 2H), 3.83 (s, 6H), 3.82 (s, 3H), 2.41 (s, 3H). ^{13}C NMR (150 MHz, $CDCl_3$) δ 197.28, 153.29, 144.16, 136.83, 134.06, 130.30, 129.38, 128.73, 106.45, 60.83, 56.09, 45.62, 21.68. ESI-HRMS (*m/z*): calcd for $C_{18}H_{20}O_4Na$ ($M + Na^+$), 323.1253; found, 323.1251.

*4.2.7. 1-(4-Methoxy-3-methylphenyl)-2-(3,4,5-trimethoxyphenyl) ethan-1-one (**3g**)*

Red solid. Yield 82%. Mp 83.4–86.2 °C.^{1}H NMR (400 MHz, $CDCl_3$) δ 7.89 (dd, J = 8.5, 1.9 Hz, 1H), 7.84 (s, 1H), 6.85 (d, J = 8.6 Hz, 1H), 6.48 (s, 2H), 4.17 (s, 2H), 3.89 (s, 3H), 3.84 (s, 6H), 3.82 (s, 3H), 2.25 (s, 3H). ^{13}C NMR (150 MHz, $CDCl_3$) δ 196.47, 161.92, 153.27, 136.77, 131.19, 130.69, 129.06, 128.84, 126.94, 109.25, 106.41, 60.83, 56.08, 55.55, 45.40, 16.32. ESI-HRMS (*m/z*): calcd for $C_{19}H_{22}O_5Na$($M + Na^+$), 353.1359; found, 353.1353.

*4.2.8. 2-(3-fluoro-4-methoxyphenyl)-1-(3,4,5-trimethoxyphenyl) ethan-1-one (**3h**)*

White solid. Yield 79%. Mp 125.3–127.8 °C.^{1}H NMR (400 MHz, DMSO) δ 7.33 (s, 2H), 7.16–7.07 (m, 2H), 7.04–7.02 (m, 1H), 4.35 (s, 2H), 3.85 (s, 6H), 3.81 (s, 3H), 3.74 (s, 3H). ^{13}C NMR (150 MHz, DMSO) δ 196.30, 152.94, 152.68, 151.87, 150.26, 145.66, 145.59, 141.82, 131.45, 128.03, 127.98, 125.74, 117.08, 116.96, 113.58, 105.90, 104.47, 60.06, 59.96, 56.01, 55.95, 55.81, 43.32. ESI-HRMS (*m/z*): calcd for $C_{18}H_{19}FO_5Na$($M + Na^+$), 357.1108; found, 357.1112.

*4.2.9. 2-(4-methoxyphenyl)-1-(3,4,5-trimethoxyphenyl)ethan-1-one (**3i**)*

White solid. Yield 83%. Mp 87.2–89.0 °C. ^{1}H NMR (400 MHz, $CDCl_3$) δ 7.26 (s, 2H), 7.19 (d, J = 8.2 Hz, 2H), 6.87 (d, J = 8.1 Hz, 2H), 4.19 (s, 2H), 3.90 (s, 3H), 3.89 (s, 6H), 3.78 (s, 3H). ^{13}C NMR (150 MHz, $CDCl_3$) δ 196.76, 158.55, 153.00, 142.52, 131.71, 130.27, 126.76, 114.20, 106.20, 60.93, 56.24, 55.25, 44.72. ESI-HRMS (*m/z*): calcd for $C_{18}H_{20}O_5Na$ ($M + Na^+$), 339.1202; found, 339.1198.

*4.2.10. 2-(benzo[d] [1,3]dioxol-5-yl)-1-(3,4,5-trimethoxyphenyl) ethan-1-one (**3j**)*

White solid. Yield 75%. Mp 98.9–101.1 °C. ^{1}H NMR (400 MHz, $CDCl_3$) δ 7.26 (s, 2H), 6.82–6.67 (m, 3H), 5.94 (s, 2H), 4.16 (s, 2H), 3.91 (s, 3H), 3.90 (s, 6H). ^{13}C NMR (150 MHz, $CDCl_3$) δ 196.50, 153.03, 147.93, 146.60, 142.62, 131.62, 128.32, 122.37, 109.69, 108.49, 106.18, 101.05, 60.95, 56.28, 45.17. ESI-HRMS (*m/z*): calcd for $C_{18}H_{18}O_6Na$ ($M + Na^+$), 353.0995; found, 353.0989.

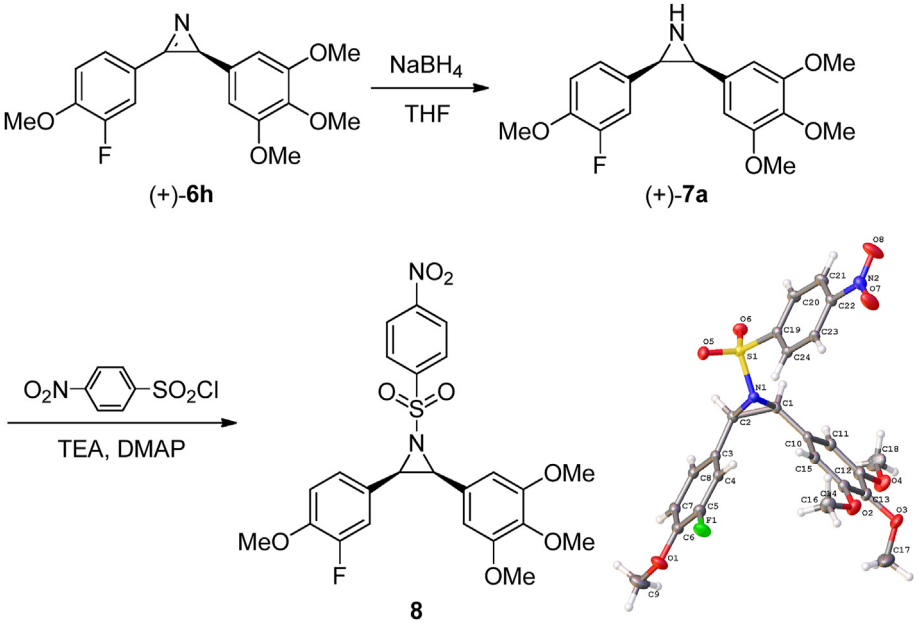

Scheme 2. Synthesis of compound **8** and its X-ray single crystal structure.

*4.2.11. 2-(3,4-dimethoxyphenyl)-1-(3,4,5-trimethoxyphenyl)ethan-1-one (**3k**)*

Yellow solid. Yield 81%. Mp 92.5–93.5 °C. ^{1}H NMR (400 MHz, $CDCl_3$) δ 7.27 (s, 2H), 6.83 (s, 2H), 6.79 (s, 1H), 4.20 (s, 2H), 3.91 (s, 3H), 3.90 (s, 6H), 3.86 (s, 6H). ^{13}C NMR (150 MHz, $CDCl_3$) δ 196.71, 153.02, 149.11, 148.04, 142.60, 131.70, 127.21, 121.43, 112.32, 111.35, 106.23, 60.95, 56.27, 55.89, 55.86, 45.20. ESI-HRMS (*m/z*): calcd for $C_{19}H_{22}O_6Na$ ($M + Na^+$), 369.1308; found, 369.1311.

*4.2.12. 2-(4-ethoxyphenyl)-1-(3,4,5-trimethoxyphenyl)ethan-1-one (**3l**)*

White solid. Yield 84%. Mp 62.8–64.9 °C. ^{1}H NMR (400 MHz, $CDCl_3$) δ 7.26 (s, 2H), 7.17 (d, J = 7.6 Hz, 2H), 6.86 (d, J = 7.4 Hz, 2H), 4.18 (s, 2H), 4.01 (q, J = 6.4 Hz, 2H), 3.90 (s, 3H), 3.89 (s, 6H), 1.40 (t, J = 6.9 Hz, 3H). ^{13}C NMR (150 MHz, $CDCl_3$) δ 196.82, 157.94, 153.00, 142.51, 131.73, 130.24, 126.62, 114.78, 106.23, 63.43, 60.94, 56.25, 44.79, 14.84. ESI-HRMS (*m/z*): calcd for $C_{19}H_{22}O_5Na$ ($M + Na^+$), 353.1359 found, 353.1357.

*4.2.13. 2-(p-tolyl)-1-(3,4,5-trimethoxyphenyl)ethan-1-one (**3m**)*

White solid. Yield 87%. Mp 75.1–76.3 °C. ^{1}H NMR (400 MHz, $CDCl_3$) δ 7.26 (s, 2H), 7.15 (dd, J = 11.6, 8.4 Hz, 4H), 4.21 (s, 2H), 3.90 (s, 3H), 3.88 (s, 6H), 2.32 (s, 3H). ^{13}C NMR (151 MHz, $CDCl_3$) δ 196.66, 152.99, 142.51, 136.55, 131.71, 129.48, 129.11, 106.24, 60.93, 56.24, 45.28, 21.07. ESI-HRMS (*m/z*): calcd for $C_{18}H_{20}O_4Na$ ($M + Na^+$), 323.1253; found, 323.1247.

*4.2.14. 2-(4-(methylthio)phenyl)-1-(3,4,5-trimethoxyphenyl)ethan-1-one (**3n**)*

Pink solid. Yield 87%. Mp 104.0–106.8 °C. ^{1}H NMR (400 MHz, $CDCl_3$) δ 7.25 (s, 2H), 7.21 (q, J = 8.3 Hz, 4H), 4.21 (s, 2H), 3.91 (s, 3H), 3.89 (s, 6H), 2.47 (s, 3H). ^{13}C NMR (151 MHz, $CDCl_3$) δ 196.33, 153.03, 142.64, 137.04, 131.61, 131.54, 129.77, 127.01, 106.19, 60.95, 56.27, 44.99, 15.92. ESI-HRMS (*m/z*): calcd for $C_{18}H_{20}O_4SNa$ ($M + Na^+$), 355.0974; found, 355.0971.

*4.2.15. 1-(Naphthalen-2-yl)-2-(3,4,5-trimethoxyphenyl)ethan-1-one (**3o**)*

Yellow oil. Yield 84%. ^{1}H NMR (400 MHz, $CDCl_3$) δ 8.55 (s, 1H), 8.06 (d, J = 8.6 Hz, 1H), 7.96 (d, J = 8.0 Hz, 1H), 7.88 (t, J = 8.9 Hz, 2H), 7.58 (m, 2H), 6.53 (s, 2H), 4.35 (s, 2H), 3.83 (d, J = 3.7 Hz, 9H).^{13}C NMR (150 MHz, $CDCl_3$) δ 197.54, 153.35, 136.91, 135.62, 133.89, 132.48, 130.35, 130.19, 129.59, 128.64, 128.57, 127.80, 126.88, 124.19, 106.52, 60.83, 56.10, 45.76.ESI-HRMS (*m/z*): calcd for $C_{21}H_{21}O_4$ ($M + H^+$), 337.1434; found, 337.1432.

*4.2.16. 1-Phenyl-2-(3,4,5-trimethoxyphenyl)ethan-1-one (**3p**)*

Yellow oil. Yield 79%. ^{1}H NMR (400 MHz, $CDCl_3$) δ 8.07–7.95 (m, 2H), 7.56 (d, J = 7.3 Hz, 1H), 7.47 (t, J = 7.5 Hz, 2H), 6.48 (s, 2H), 4.22 (s, 2H), 3.83 (s, 6H), 3.83 (s, 3H).^{13}C NMR (150 MHz, $CDCl_3$) δ 197.59, 153.33, 136.90, 136.57, 133.29, 130.04, 128.69, 128.57, 106.47, 60.83, 56.09, 45.71.ESI-HRMS (*m/z*): calcd for $C_{17}H_{19}O_4$ ($M + H^+$), 287.1278; found, 287.1275.

*4.2.17. 2-(Naphthalen-2-yl)-1-(3,4,5-trimethoxyphenyl)ethan-1-one (**3q**)*

Yellow oil. Yield 87%.^{1}H NMR (400 MHz, $CDCl_3$) δ 7.80 (m, 3H), 7.72 (s, 1H), 7.50–7.42 (m, 2H), 7.40 (d, J = 8.4 Hz, 1H), 7.30 (s, 1H), 4.41 (s, 2H), 3.89 (s, 3H), 3.88 (s, 6H).^{13}C NMR (150 MHz, $CDCl_3$) δ 196.44, 153.03, 142.62, 133.57, 132.36, 131.67, 128.42, 127.94, 127.68, 127.57, 127.40, 126.21, 125.80, 106.27, 60.93, 56.25, 45.81.ESI-HRMS (*m/z*): calcd for $C_{21}H_{21}O_4$ ($M + H^+$), 337.1434; found, 337.1432.

*4.2.18. 2-Phenyl-1-(3,4,5-trimethoxyphenyl)ethan-1-one(**3r**)*

Yellow oil. Yield 81%.^{1}H NMR (400 MHz, $CDCl_3$) δ 7.33 (t, J = 7.2 Hz, 2H), 7.29–7.22 (m, 5H), 4.25 (s, 2H), 3.90 (s, 3H), 3.88 (s, 6H).^{13}C NMR (150 MHz, $CDCl_3$) δ 196.45, 153.01, 142.57, 134.84, 131.69, 129.27, 128.76, 126.94, 106.24, 60.93, 56.24, 45.65.ESI-HRMS (*m/z*): calcd for $C_{17}H_{19}O_4$ ($M + H^+$), 287.1278; found, 287.1279.

*4.3. General procedure for the synthesis of ketoximes (**4a**-**r**)*

The mixture of diaryl ethyl ketone **3** (3 mmol), hydroxylamine hydrochloride (4.5 mmol) and potassium carbonate (6 mmol) in anhydrous methanol (20 mL) was heated at 50 °C until starting materials (**3a**-**r**) had been completely consumed. The solvent was removed under reduced pressure and the residue was directly purified by flash column chromatography to give the title compound **4**.

*4.3.1. 1-(3-fluoro-4-methoxyphenyl)-2-(3,4,5-trimethoxyphenyl) ethan-1-one oxime (**4a**)*

White solid. Yield 86%. Mp 123.5–126.0 °C. ^{1}H NMR (400 MHz, $CDCl_3$) δ 7.43 (d, J = 12.6 Hz, 1H), 7.34 (d, J = 7.6 Hz, 1H), 6.91 (t, J = 8.6 Hz, 1H), 6.46 (s, 2H), 4.10 (s, 2H), 3.89 (s, 3H), 3.80 (d, J = 2.6 Hz, 9H). ^{13}C NMR (150 MHz, $CDCl_3$) δ 156.16, 153.34, 152.99, 151.36, 148.68, 148.61, 136.58, 131.90, 128.65, 128.61, 122.71, 114.16, 114.03, 112.90, 105.40, 60.85, 56.20, 56.08, 31.97. ESI-HRMS (*m/z*): calcd for $C_{18}H_{20}FNO_5Na$ ($M + Na^+$), 372.1223; found, 372.1228.

*4.3.2. 1-(4-methoxyphenyl)-2-(3,4,5-trimethoxyphenyl)ethan-1-one oxime (**4b**)*

Yellow oil. Yield 82%. ^{1}H NMR (600 MHz, $CDCl_3$) δ 7.57 (d, J = 8.9 Hz, 2H), 6.87 (d, J = 8.9 Hz, 2H), 6.47 (s, 2H), 4.12 (s, 2H), 3.81 (s, 3H), 3.80 (s, 3H), 3.79 (s, 6H). ^{13}C NMR (150 MHz, $CDCl_3$) δ 160.55, 157.10, 153.28, 136.50, 132.27, 128.14, 127.87, 113.94, 105.50, 60.83, 56.06, 55.30, 32.22. ESI-HRMS (*m/z*): calcd for $C_{18}H_{21}NO_5Na$ ($M + Na^+$), 354.1317; found, 354.1313.

*4.3.3. 1-(benzo[d] [1,3]dioxol-5-yl)-2-(3,4,5-trimethoxyphenyl) ethan-1-one oxime (**4c**)*

White solid. Yield 83%. Mp 143.3–146.6 °C. ^{1}H NMR (400 MHz, $CDCl_3$) δ 7.17 (s, 1H), 7.10 (d, J = 7.9 Hz, 1H), 6.78 (d, J = 8.0 Hz, 1H), 6.47 (s, 2H), 5.97 (s, 2H), 4.10 (s, 2H), 3.80 (s, 9H). ^{13}C NMR (150 MHz, $CDCl_3$) δ 157.04, 153.30, 148.68, 147.96, 136.54, 132.12, 129.81, 120.91, 108.15, 106.62, 105.45, 101.34, 60.84, 56.09, 32.30. ESI-HRMS (*m/z*): calcd for $C_{18}H_{19}NO_6Na$ ($M + Na^+$), 368.1104; found, 368.1101.

*4.3.4. 1-(3,4-dimethoxyphenyl)-2-(3,4,5-trimethoxyphenyl)ethan-1-one oxime (**4d**)*

Yellow solid. Yield 78%. Mp 118.2–120.6 °C. ^{1}H NMR (400 MHz, $CDCl_3$) δ 7.88 (s, 1H), 7.29 (d, J = 1.9 Hz, 1H), 7.15 (dd, J = 8.4, 2.0 Hz, 1H), 6.83 (d, J = 8.4 Hz, 1H), 6.49 (s, 2H), 4.12 (s, 2H), 3.89 (s, 3H), 3.88 (s, 3H), 3.80 (s, 3H), 3.80 (s, 6H). ^{13}C NMR (150 MHz, $CDCl_3$) δ 157.15, 153.29, 150.21, 148.90, 136.49, 132.44, 128.36, 119.72, 110.60, 108.92, 105.46, 60.85, 56.07, 55.89, 55.84, 32.10, 29.33. ESI-HRMS (*m/z*): calcd for $C_{19}H_{23}NO_6Na$ ($M + Na^+$), 384.1416; found, 384.1417.

*4.3.5. 1-(4-ethoxyphenyl)-2-(3,4,5-trimethoxyphenyl)ethan-1-one oxime (**4e**)*

Red solid. Yield 86%. Mp 112.1–115.3 °C. ^{1}H NMR (400 MHz, $CDCl_3$) δ 7.56 (d, J = 8.6 Hz, 2H), 6.86 (d, J = 8.6 Hz, 2H), 6.48 (s, 2H), 4.13 (s, 2H), 4.03 (q, J = 7.0 Hz, 2H), 3.80 (s, 3H), 3.78 (s, 6H), 1.41 (t, J = 6.9 Hz, 3H). ^{13}C NMR (150 MHz, $CDCl_3$) δ 159.94, 157.04, 153.25, 136.44, 132.28, 127.91, 127.84, 114.45, 105.47, 63.50, 60.83, 56.05, 32.26, 14.75. ESI-HRMS (*m/z*): calcd for $C_{19}H_{23}NO_5Na$ ($M + Na^+$), 368.1468; found, 368.1469.

*4.3.6. 1-(p-tolyl)-2-(3,4,5-trimethoxyphenyl)ethan-1-one oxime (**4f**)*

Yellow solid. Yield 79%. Mp 124.1–126.9 °C. ^{1}H NMR (400 MHz, $CDCl_3$) δ 7.52 (d, J = 8.2 Hz, 2H), 7.16 (d, J = 8.0 Hz, 2H), 6.47 (s, 2H), 4.14 (s, 2H), 3.80 (s, 3H), 3.78 (s, 6H), 2.35 (s, 3H). ^{13}C NMR (150 MHz, $CDCl_3$) δ 157.43, 153.24, 139.48, 136.45, 132.80, 132.20, 129.28, 126.38, 105.48,60.83, 56.22, 56.04, 32.29, 21.27. ESI-HRMS (m/z): calcd for $C_{18}H_{21}NO_4Na$ (M + Na^+), 338.1362; found, 338.1360.

*4.3.7. 1-(4-Methoxy-3-methylphenyl)-2-(3,4,5-trimethoxyphenyl) ethan-1-one oxime (**4g**)*

Yellow solid. Yield 85%. Mp 117.1–120.4 °C. ^{1}H NMR (400 MHz, $CDCl_3$) δ 7.46 (s, 1H), 7.42 (dd, J = 8.5, 2.1 Hz, 1H), 6.78 (d, J = 8.5 Hz, 1H), 6.49 (s, 2H), 4.13 (s, 2H), 3.83 (s, 3H), 3.80 (s, 3H), 3.79 (s, 6H), 2.20 (s, 3H). ^{13}C NMR (150 MHz, $CDCl_3$) δ 158.82, 157.22, 153.23, 136.42, 132.41, 128.63, 127.57, 126.80, 125.43, 109.63, 105.49, 60.83, 56.04, 55.35, 32.26, 16.37. ESI-HRMS (m/z): calcd for $C_{19}H_{23}NO_5Na$ (M + Na^+),368.1468; found,368.1459.

*4.3.8. 2-(3-fluoroxyphenyl)etha-4-methoxyphenyl)-1-(3,4,5-trimethon-1-one oxime (**4h**)*

White solid. Yield 85%. Mp 96.9–99.1 °C. ^{1}H NMR (400 MHz, $CDCl_3$) δ 7.04 (d, J = 12.2 Hz, 1H), 6.97 (d, J = 8.2 Hz, 1H), 6.87 (d, J = 9.1 Hz, 1H), 6.84 (s, 2H), 4.10 (s, 2H), 3.85 (d, J = 2.6 Hz, 6H), 3.83 (s, 6H). ^{13}C NMR (150 MHz, $CDCl_3$) δ 157.09, 153.18, 151.54, 146.23, 146.16, 139.27, 130.83, 129.59, 129.55, 124.14, 124.12, 116.46, 116.34, 113.51, 103.84, 60.90, 56.28, 56.14, 31.29. ESI-HRMS (m/z): calcd for $C_{18}H_{20}FNO_5Na$ (M + Na^+), 372.1217; found, 372.1216.

*4.3.9. 2-(4-methoxyphenyl)-1-(3,4,5-trimethoxyphenyl)ethan-1-one oxime (**4i**)*

White solid. Yield 72%. Mp 123.4–125.3 °C. ^{1}H NMR (400 MHz, $CDCl_3$) δ 8.97 (s, 1H), 7.19 (d, J = 7.7 Hz, 2H), 6.85 (s, 2H), 6.81 (d, J = 7.5 Hz, 2H), 4.11 (s, 2H), 3.84 (s, 3H), 3.81 (s, 6H), 3.76 (s, 3H). ^{13}C NMR (150 MHz, $CDCl_3$) δ 158.16, 157.62, 153.10, 139.08, 131.14, 129.53, 128.65, 114.08, 103.90, 60.88, 56.10, 55.24, 31.41. ESI-HRMS (m/z): calcd for $C_{18}H_{21}NO_5Na$ (M + Na^+), 354.1311; found, 354.1305.

*4.3.10. 2-(benzo[d] [1,3]dioxol-5-yl)-1-(3,4,5-trimethoxyphenyl) ethan-1-one oxime (**4j**)*

White solid. Yield 76%. Mp 96.3–98.7 °C. ^{1}H NMR (400 MHz, $CDCl_3$) δ 8.17 (s, 1H), 6.86 (s, 2H), 6.78 (s, 1H), 6.73 (s, 2H), 5.91 (s, 2H), 4.09 (s, 2H), 3.85 (s, 3H), 3.83 (s, 6H). ^{13}C NMR (150 MHz, $CDCl_3$) δ 157.44, 153.12, 147.91, 146.14, 139.16, 130.97, 130.36, 121.46, 109.07, 108.34, 103.86, 100.94, 60.89, 56.13, 31.73. ESI-HRMS (m/z): calcd for $C_{18}H_{19}NO_6Na$ (M + Na^+), 368.1104; found, 368.1109.

*4.3.11. 2-(3,4-dimethoxyphenyl)-1-(3,4,5-trimethoxyphenyl)ethan-1-one oxime (**4k**)*

White solid. Yield 83%. Mp 137.4–139.9 °C. ^{1}H NMR (400 MHz, cdcl$_3$) δ 8.73 (s, 1H), 6.86 (s, 2H), 6.83 (s, 1H), 6.79 (d, J = 5.6 Hz, 2H), 4.12 (s, 2H), 3.84 (s, 6H), 3.81 (s, 9H). ^{13}C NMR (150 MHz, $CDCl_3$) δ 157.58, 153.11, 149.06, 147.65, 139.13, 131.22, 129.16, 120.49, 111.86, 111.28, 103.93, 60.89, 56.12, 55.88, 55.81, 31.86. ESI-HRMS (m/z): calcd for $C_{19}H_{23}NO_6Na$ (M + Na^+), 384.1417; found, 384.1421.

*4.3.12. 2-(4-ethoxyphenyl)-1-(3,4,5-trimethoxyphenyl)ethan-1-one oxime (**4l**)*

White solid. Yield 81%. Mp 148.0–150.3 °C. ^{1}H NMR (400 MHz, $CDCl_3$) δ 9.01 (s, 1H), 7.18 (d, J = 8.6 Hz, 2H), 6.85 (s, 2H), 6.80 (d, J = 8.7 Hz, 2H), 4.11 (s, 2H), 3.98 (q, J = 7.0 Hz, 2H), 3.84 (s, 3H), 3.80 (s, 6H), 1.38 (t, J = 7.0 Hz, 3H). ^{13}C NMR (150 MHz, $CDCl_3$) δ 157.63, 157.53, 153.08, 139.06, 131.17, 129.51, 128.51, 114.65, 103.90, 63.40, 60.88, 56.09, 31.45, 14.84. ESI-HRMS (m/z): calcd for $C_{19}H_{23}NO_5Na$ (M + Na^+), 368.1468; found, 368.1469.

*4.3.13. 2-(p-tolyl)-1-(3,4,5-trimethoxyphenyl)ethan-1-one oxime (**4m**)*

Colorless oil. Yield 86%. ^{1}H NMR (400 MHz, $CDCl_3$) δ 7.16 (d, J = 8.0 Hz, 2H), 7.08 (d, J = 7.9 Hz, 2H), 6.86 (s, 2H), 4.14 (s, 2H), 3.84 (s, 3H), 3.81 (s, 6H), 2.30 (s, 3H). ^{13}C NMR (150 MHz, $CDCl_3$) δ 157.50, 153.09, 139.08, 135.98, 133.59, 131.14, 129.36, 128.38, 103.88, 60.87, 60.44, 56.09, 31.82, 21.07, 21.02, 14.20. ESI-HRMS (m/z): calcd for $C_{18}H_{21}NO_4Na$ (M + Na^+), 338.1362; found, 338.1360.

*4.3.14. 2-(4-(methylthio)phenyl)-1-(3,4,5-trimethoxyphenyl) ethan-1-one oxime (**4n**)*

White solid. Yield 79%. Mp 95.6–98.9 °C. ^{1}H NMR (400 MHz, $CDCl_3$) δ 7.19 (m, 4H), 6.84 (s, 2H), 4.13 (s, 2H), 3.84 (s, 3H), 3.81 (s, 6H), 2.45 (s, 3H). ^{13}C NMR (150 MHz, $CDCl_3$) δ 157.24, 153.13, 139.19, 136.31, 133.59, 130.94, 129.02, 127.10, 103.87, 60.89, 56.12, 31.68, 16.02. ESI-HRMS (m/z): calcd for $C_{18}H_{21}NO_4SNa$ (M + Na^+), 370.1083; found, 370.1081.

*4.3.15. 1-(Naphthalen-2-yl)-2-(3,4,5-trimethoxyphenyl)ethan-1-one oxime (**4o**)*

Colourless oil. Yield 73%. ^{1}H NMR (400 MHz, $CDCl_3$) δ 8.04 (s, 1H), 7.84 (m, 4H), 7.55–7.44 (m, 2H), 6.53 (s, 2H), 4.27 (s, 2H), 3.80 (s, 3H), 3.78 (s, 6H).^{13}C NMR (150 MHz, $CDCl_3$) δ 157.54, 153.32, 136.52, 133.70, 133.05, 132.98, 132.19, 128.50, 128.27, 127.65, 126.82, 126.49, 126.45, 123.65, 105.48, 105.00, 60.83, 56.22, 56.06, 32.11.ESI-HRMS (m/z): calcd for $C_{21}H_{22}NO_4$ (M + H^+), 352.1543; found, 352.1537.

*4.3.16. 1-Phenyl-2-(3,4,5-trimethoxyphenyl)ethan-1-one oxime (**4p**)*

Yellow oil. Yield 77%. ^{1}H NMR (400 MHz, $CDCl_3$) δ 7.67–7.57 (m, 2H), 7.36 (s, 3H), 6.47 (s, 2H), 4.15 (s, 2H), 3.80 (s, 3H), 3.78 (s, 6H).^{13}C NMR (150 MHz, $CDCl_3$) δ 157.50, 153.25, 136.49, 135.68, 132.03, 129.39, 128.56, 126.51, 105.49, 60.83, 56.04, 32.39.ESI-HRMS (m/z): calcd for $C_{17}H_{20}NO_4$ (M + H^+), 302.1387; found, 302.1385.

*4.3.17. 2-(Naphthalen-2-yl)-1-(3,4,5-trimethoxyphenyl)ethan-1-one oxime (**4q**)*

Yellow oil. Yield 79%. ^{1}H NMR (400 MHz, $CDCl_3$) δ 7.74 (m, 4H), 7.43 (s, 3H), 6.90 (s, 2H), 4.34 (s, 2H), 3.82 (s, 3H), 3.77 (s, 6H).^{13}C NMR (150 MHz, $CDCl_3$) δ 157.26, 153.13, 139.17, 134.22, 133.61, 132.17, 131.05, 128.36, 127.62, 127.49, 126.98, 126.85, 126.12, 125.55, 103.92, 60.86, 56.08, 32.47.ESI-HRMS (m/z): calcdfor $C_{21}H_{22}NO_4$ (M + H^+), 352.1543; found, 352.1540.

*4.3.18. 2-Phenyl-1-(3,4,5-trimethoxyphenyl)ethan-1-one oxime (**4r**)*

Yellow oil. Yield 75%. ^{1}H NMR (400 MHz, $CDCl_3$) δ 7.27 (t, J = 4.6 Hz, 4H), 7.20 (dd, J = 8.2, 4.0 Hz, 1H), 6.85 (s, 2H), 4.18 (s, 2H), 3.84 (s, 3H), 3.80 (s, 6H).^{13}C NMR (150 MHz, $CDCl_3$) δ 157.30, 153.10, 139.12, 136.73, 131.07, 128.68, 128.52, 126.46, 103.89, 60.88, 56.08, 32.31.ESI-HRMS (m/z): calcd for $C_{17}H_{20}NO_4$ (M + H^+), 302.1387; found, 302.1386.

*4.4. General procedure for the synthesis of 2H-azirines (**6a**-**r**)*

A solution of ketoxime **4a**-**r** (1 mmol), acetic anhydride (1.5 mmol) and triethylamine (2 mmol) in dichloromethane (15 mL) was stirred at room temperature for 30 min. Water (20 mL) was then added into the solution, and the mixture was extracted with dichloromethane (10 mL) for 3 times. The organic layer was separated, washed with brine, dried over anhydrous sodium sulfate and filtered. After removing the solvent, the crude ketoxime acetates **5a**-**r** were used directly for the next step.

Under a nitrogen atmosphere, ketoxime acetate **5a**-**r** (0.5 mmol)

and cesium carbonate (1 mmol) were stirred in *N*,*N*-dimethylformamide (DMF, 10 mL) at 80 °C for 1 h. The reaction mixture was then cooled to room temperature, extracted with ethyl acetate (15 mL) for 3 times and washed with brine (15 mL). The combined organic layer was dried over anhydrous sodium sulfate and concentrated in vacuo. The residue was purified by flash column chromatography to afford corresponding compounds **6a**-**r**.

4.4.1. 3-(3-fluoro-4-methoxyphenyl)-2-(3,4,5-trimethoxyphenyl)-2H-azirine (**6a**)

Yellow solid. Yield 78%. Mp 121.1–123.8 °C. ^{1}H NMR (400 MHz, $CDCl_3$) δ 7.66 (d, J = 9.5 Hz, 2H), 7.11 (t, J = 7.9 Hz, 1H), 6.34 (s, 2H), 3.98 (s, 3H), 3.81 (s, 9H), 3.24 (s, 1H). ^{13}C NMR (150 MHz, $CDCl_3$) δ 162.43, 153.34, 153.27, 151.98, 151.91, 151.62, 137.32, 136.46, 127.31, 116.91, 116.79, 116.65, 116.60, 113.40, 102.78, 60.88, 56.38, 56.06, 34.93. ESI-HRMS (*m/z*): calcd for $C_{18}H_{18}FNO_4Na$ (M + Na^+), 354.1118; found, 354.1113.

4.4.2. 3-(4-methoxyphenyl)-2-(3,4,5-trimethoxyphenyl)-2H-azirine (**6b**)

Yellow solid. Yield 71%. Mp 117.5–120.6 °C. ^{1}H NMR (400 MHz, $CDCl_3$) δ 7.86 (d, J = 8.2 Hz, 2H), 7.06 (d, J = 8.2 Hz, 2H), 6.35 (s, 2H), 3.90 (s, 3H), 3.81 (s, 3H), 3.80 (s, 6H), 3.21 (s, 1H). ^{13}C NMR (150 MHz, $CDCl_3$) δ 163.58, 162.38, 153.29, 137.15, 137.02, 131.91, 116.28, 114.81, 102.75, 60.87, 56.05, 55.58, 34.41. ESI-HRMS (*m/z*): calcd for $C_{18}H_{19}NO_4Na$ (M + Na^+), 336.1212; found, 336.1204.

4.4.3. 3-(benzo[d] [1,3]dioxol-5-yl)-2-(3,4,5-trimethoxyphenyl)-2H-azirine (**6c**)

Yellow solid. Yield 79%. Mp 113.6–115.5 °C. ^{1}H NMR (400 MHz, $CDCl_3$) δ 7.40 (s, 2H), 6.96 (d, J = 7.1 Hz, 1H), 6.34 (s, 2H), 6.10 (s, 2H), 3.81 (s, 9H), 3.22 (s, 1H), 1.65 (s, 2H). ^{13}C NMR (150 MHz, $CDCl_3$) δ 162.73, 153.30, 152.01, 148.59, 137.22, 136.71, 126.38, 117.82, 109.04, 108.69, 102.76, 102.09, 60.87, 56.05, 34.93. ESI-HRMS (*m/z*): calcd for $C_{18}H_{17}NO_5Na$ (M + Na^+), 350.1004; found, 350.0990.

4.4.4. 3-(3,4-dimethoxyphenyl)-2-(3,4,5-trimethoxyphenyl)-2H-azirine (**6d**)

Yellow solid. Yield 75%. Mp 101.5–103.6 °C. ^{1}H NMR (400 MHz, $CDCl_3$) δ 7.48 (d, J = 8.6 Hz, 1H), 7.43 (dd, J = 8.2, 1.7 Hz, 1H), 6.99 (d, J = 8.3 Hz, 1H), 6.36 (s, 2H), 3.97 (s, 6H), 3.82 (s, 3H), 3.81 (s, 6H), 3.24 (s, 1H). ^{13}C NMR (150 MHz, $CDCl_3$) δ 162.81, 153.32, 153.26, 149.69, 137.23, 136.92, 124.83, 116.41, 111.06, 110.91, 102.85, 60.89, 56.18, 56.16, 56.07, 34.97. ESI-HRMS (*m/z*): calcd for $C_{19}H_{21}NO_5Na$ (M + Na^+), 366.1317; found, 366.1312.

4.4.5. 3-(4-ethoxyphenyl)-2-(3,4,5-trimethoxyphenyl)-2H-azirine (**6e**)

Yellow solid. Yield 81%. Mp 99.8–102.1 °C. ^{1}H NMR (400 MHz, $CDCl_3$) δ 7.84 (d, J = 8.6 Hz, 2H), 7.04 (d, J = 8.6 Hz, 2H), 6.35 (s, 2H), 4.12 (q, J = 6.9 Hz, 2H), 3.81 (s, 3H), 3.80 (s, 6H), 3.20 (s, 1H), 1.46 (t, J = 6.9 Hz, 3H). ^{13}C NMR (150 MHz, $CDCl_3$) δ 163.00, 162.34, 153.28, 137.13, 137.07, 131.91, 116.03, 115.22, 102.74, 63.90, 60.87, 56.04, 34.37, 14.66. ESI-HRMS (*m/z*): calcd for $C_{19}H_{21}NO_4Na$ (M + Na^+), 350.1368; found, 350.1364.

4.4.6. 3-(p-tolyl)-2-(3,4,5-trimethoxyphenyl)-2H-azirine (**6f**)

Yellow solid. Yield 73%. Mp 79.8–82.6 °C. ^{1}H NMR (400 MHz, $CDCl_3$) δ 7.81 (d, J = 7.9 Hz, 2H), 7.37 (d, J = 7.8 Hz, 2H), 6.35 (s, 2H), 3.81 (s, 3H), 3.80 (s, 6H), 3.23 (s, 1H), 2.46 (s, 3H). ^{13}C NMR (150 MHz, $CDCl_3$) δ 163.26, 153.30, 144.22, 137.21, 136.86, 130.04, 129.92, 121.16, 102.79, 60.87, 56.05, 34.55, 21.92. ESI-HRMS (*m/z*): calcd for $C_{18}H_{19}NO_3Na$ (M + Na^+), 320.1257; found, 320.1250.

4.4.7. 3-(4-Methoxy-3-methylphenyl)-2-(3,4,5-trimethoxyphenyl)-2H-azirine (**6g**)

Yellow solid. Yield 67%. Mp 96.6–98.8 °C. ^{1}H NMR (400 MHz, $CDCl_3$) δ 7.73 (d, J = 8.7 Hz, 1H), 7.70 (s, 1H), 6.96 (d, J = 8.3 Hz, 1H), 6.35 (s, 2H), 3.92 (s, 3H), 3.81 (s, 3H), 3.81 (s, 6H), 3.19 (s, 1H), 2.27 (s, 3H). ^{13}C NMR (151 MHz, $CDCl_3$) δ 162.36, 161.83, 153.28, 137.22, 137.10, 131.98, 129.91, 128.08, 115.64, 110.21, 102.75, 60.87, 56.05, 55.61, 34.37, 16.18. ESI-HRMS (*m/z*): calcd for $C_{19}H_{21}NO_4Na$ (M + Na^+), 350.1362; found, 350.1357.

4.4.8. 2-(3-fluoro-4-methoxyphenyl)-3-(3,4,5-trimethoxyphenyl)-2H-azirine (**6h**)

Yellow solid. Yield 78%. Mp 84.3–86.5 °C. ^{1}H NMR (400 MHz, $CDCl_3$) δ 7.12 (s, 1H), 6.91 (s, 1H), 6.90 (d, J = 11.9 Hz, 1H), 6.84 (d, J = 11.9 Hz, 1H), 3.95 (s, 3H), 3.92 (s, 6H), 3.87 (s, 3H), 3.28 (s, 1H). ^{13}C NMR (150 MHz, $CDCl_3$) δ 163.28, 153.89, 153.25, 151.62, 146.99, 146.91, 142.33, 134.14, 134.10, 121.97, 118.84, 113.87, 113.74, 113.37, 106.74, 61.05, 56.39, 34.3. ESI-HRMS (*m/z*): calcd for $C_{18}H_{18}FNO_4Na$ (M + Na^+), 354.1112; found, 354.1107.

4.4.9. 2-(4-methoxyphenyl)-3-(3,4,5-trimethoxyphenyl)-2H-azirine (**6i**)

Yellow solid. Yield 72%. Mp 88.8–91.5 °C. ^{1}H NMR (400 MHz, $CDCl_3$) δ 7.14 (s, 2H), 7.09 (d, J = 7.8 Hz, 2H), 6.84 (d, J = 7.8 Hz, 2H), 3.94 (s, 3H), 3.91 (s, 6H), 3.79 (s, 3H), 3.32 (s, 1H). ^{13}C NMR (150 MHz, $CDCl_3$) δ 163.80, 159.04, 153.84, 142.11, 132.89, 127.38, 119.38, 113.87, 106.64, 61.04, 56.38, 55.33, 34.84. ESI-HRMS (*m/z*): calcd for $C_{18}H_{19}NO_4Na$ (M + Na^+), 336.1206; found, 336.1208.

4.4.10. 2-(benzo[d] [1,3]dioxol-5-yl)-3-(3,4,5-trimethoxyphenyl)-2H-azirine (**6j**)

Yellow solid. Yield 68%. Mp 89.2–91.5 °C. ^{1}H NMR (400 MHz, $CDCl_3$) δ 7.13 (s, 2H), 6.73 (m, 2H), 6.56 (s, 1H), 5.93 (s, 2H), 3.94 (s, 3H), 3.92 (s, 6H), 3.29 (s, 1H). ^{13}C NMR (150 MHz, $CDCl_3$) δ 163.69, 153.86, 147.86, 147.00, 142.21, 134.96, 119.84, 119.11, 108.22, 106.69, 106.39, 101.05, 61.04, 56.39, 35.17. ESI-HRMS (*m/z*): calcd for $C_{18}H_{17}NO_5Na$ (M + Na^+), 350.0998; found, 350.0991.

4.4.11. 2-(3,4-dimethoxyphenyl)-3-(3,4,5-trimethoxyphenyl)-2H-azirine (**6k**)

Yellow solid. Yield 77%. Mp 121.5–124.7 °C. ^{1}H NMR (400 MHz, $CDCl_3$) δ 7.14 (s, 2H), 6.82 (d, J = 8.0 Hz, 1H), 6.74 (d, J = 7.7 Hz, 1H), 6.66 (s, 1H), 3.94 (s, 3H), 3.92 (s, 6H), 3.87 (s, 3H), 3.84 (s, 3H), 3.31 (s, 1H). ^{13}C NMR (150 MHz, $CDCl_3$) δ 163.78, 153.85, 149.01, 148.49, 142.17, 133.44, 119.26, 118.56, 111.18, 109.18, 106.67, 61.04, 56.39, 55.99, 55.89, 35.16. ESI-HRMS (*m/z*): calcd for $C_{19}H_{21}NO_5Na$ (M + Na^+), 366.1311; found, 366.1312.

4.4.12. 2-(4-ethoxyphenyl)-3-(3,4,5-trimethoxyphenyl)-2H-azirine (**6l**)

Yellow solid. Yield 74%. Mp 103.1–105.7 °C. ^{1}H NMR (400 MHz, $CDCl_3$) δ 7.14 (s, 2H), 7.08 (d, J = 8.6 Hz, 2H), 6.83 (d, J = 8.6 Hz, 2H), 4.01 (q, J = 7.0 Hz, 2H), 3.94 (s, 3H), 3.91 (s, 6H), 3.31 (s, 1H), 1.40 (t, J = 7.0 Hz, 3H). ^{13}C NMR (150 MHz, $CDCl_3$) δ 163.83, 158.41, 153.84, 142.09, 132.72, 127.38, 119.43, 114.44, 106.63, 63.50, 61.04, 56.39, 34.89, 14.83. ESI-HRMS (*m/z*): calcd for $C_{19}H_{21}NO_4Na$ (M + Na^+), 350.1362; found, 350.1354.

4.4.13. 2-(p-tolyl)-3-(3,4,5-trimethoxyphenyl)-2H-azirine (**6m**)

Yellow solid. Yield 80%. Mp 89.6–92.4 °C. ^{1}H NMR (400 MHz, $CDCl_3$) δ 7.14 (s, 2H), 7.11 (d, J = 8.0 Hz, 1H), 7.06 (d, J = 8.1 Hz, 1H), 3.94 (s, 3H), 3.91 (s, 6H), 3.32 (s, 1H), 2.33 (s, 3H). ^{13}C NMR (150 MHz, $CDCl_3$) δ 163.44, 153.83, 142.13, 137.84, 136.92, 129.05, 126.18, 119.28, 106.70, 61.04, 56.38, 35.08, 21.14. ESI-HRMS (*m/z*): calcd for $C_{18}H_{19}NO_3Na$ (M + Na^+), 320.1257; found, 320.1254.

4.4.14. 2-(4-(methylthio)phenyl)-3-(3,4,5-trimethoxyphenyl)-2H-azirine (**6n**)

Yellow solid. Yield 71%. Mp 84.7–86.0 °C. ^{1}H NMR (400 MHz, $CDCl_3$) δ 7.20 (d, J = 8.3 Hz, 2H), 7.13 (s, 2H), 7.09 (d, J = 8.3 Hz, 2H), 3.94 (s, 3H), 3.91 (s, 6H), 3.31 (s, 1H), 2.47 (s, 3H). ^{13}C NMR (150 MHz, $CDCl_3$) δ 163.28, 153.86, 142.25, 137.92, 137.22, 126.72, 119.01, 106.73, 61.05, 56.40, 34.84, 16.05. ESI-HRMS (m/z): calcd for $C_{18}H_{19}NO_3SNa$ ($M + Na^+$), 352.0977; found, 352.0981.

4.4.15. 3-(Naphthalen-2-yl)-2-(3,4,5-trimethoxyphenyl)-2H-azirine (**6o**)

Yellow oil. Yield 67%. ^{1}H NMR (400 MHz, $CDCl_3$) δ 8.32 (s, 1H), 8.03 (q, J = 8.5 Hz, 2H), 7.93 (t, J = 6.9 Hz, 2H), 7.60 (m, 2H), 6.41 (s, 2H), 3.82 (s, 3H), 3.80 (s, 6H), 3.35 (s, 1H).^{13}C NMR (150 MHz, $CDCl_3$) δ 191.09, 163.79, 153.64, 153.36, 137.32, 136.67, 135.62, 132.84, 132.05, 129.39, 129.08, 128.75, 128.11, 127.23, 124.56, 121.23, 106.70, 102.87, 60.87, 56.05, 35.05.ESI-HRMS (m/z): calcd for $C_{21}H_{20}NO_3$ ($M + H^+$), 334.1438; found, 334.1435.

4.4.16. 3-Phenyl-2-(3,4,5-trimethoxyphenyl)-2H-azirine (**6p**)

Yellow oil. Yield 64%. ^{1}H NMR (400 MHz, $CDCl_3$) δ 7.92 (d, J = 7.0 Hz, 2H), 7.66–7.48 (m, 3H), 6.36 (s, 2H), 3.82 (s, 3H), 3.80 (s, 6H), 3.26 (s, 1H).^{13}C NMR (150 MHz, $CDCl_3$) δ 163.80, 153.32, 137.29, 136.61, 133.29, 129.88, 129.29, 124.00, 102.81, 60.86, 56.05, 34.79.ESI-HRMS (m/z): calcd for $C_{17}H_{18}NO_3$ ($M + H^+$), 284.1281; found, 284.1279.

4.4.17. 2-(Naphthalen-2-yl)-3-(3,4,5-trimethoxyphenyl)-2H-azirine (**6q**)

Yellow oil. Yield 76%. ^{1}H NMR (400 MHz, $CDCl_3$) δ 7.86–7.72 (m, 3H), 7.67 (s, 1H), 7.45 (d, J = 6.1 Hz, 2H), 7.23 (d, J = 8.5 Hz, 1H), 7.17 (s, 2H), 3.94 (s, 3H), 3.90 (s, 6H), 3.50 (s, 1H).^{13}C NMR (150 MHz, $CDCl_3$) δ 163.21, 153.88, 142.28, 138.44, 133.25, 132.79, 128.08, 127.73, 127.53, 126.30, 125.62, 125.05, 124.08, 119.05, 106.82, 61.04, 56.37, 35.41.ESI-HRMS (m/z): calcd for $C_{21}H_{20}NO_3$ ($M + H^+$), 334.1438; found, 334.1435.

4.4.18. 2-Phenyl-3-(3,4,5-trimethoxyphenyl)-2H-azirine (**6r**)

Yellow oil. Yield 73%. ^{1}H NMR (400 MHz, $CDCl_3$) δ 7.34–7.21 (m, 3H), 7.20–7.15 (m, 2H), 7.14 (s, 2H), 3.94 (d, J = 1.6 Hz, 3H), 3.90 (d, J = 1.6 Hz, 6H), 3.33 (s, 1H).^{13}C NMR (150 MHz, $CDCl_3$) δ 163.12, 153.85, 142.21, 140.89, 128.33, 127.15, 126.23, 119.08, 106.76, 61.03, 56.39, 35.17.ESI-HRMS (m/z): calcd for $C_{17}H_{18}NO_3$($M + H^+$), 284.1281; found, 284.1279.

4.5. Procedure for the synthesis ofaziridinederivatives

4.5.1. 2-(3-fluoro-4-methoxyphenyl)-3-(3,4,5-trimethoxyphenyl) aziridine (**7a**)

A mixture of **6h** (23 mg, 0.069 mmol) and sodium borohydride (10 mg, 0.278 mmol) in tetrahydrofuran (1.5 mL) was stirred at room temperature for 2 h. The solvent was removed under reduced pressure and the residue was directly purified by flash column chromatography (elute with ethyl acetate/hexane = 2:1, v/v) to give the title compound **7a** as yellow solid (21 mg, yield 91%), Mp 117.4–120.3 °C. ^{1}H NMR (400 MHz, $CDCl_3$) δ 6.99 (dd, J = 12.4, 1.8 Hz, 1H), 6.91 (d, J = 8.4 Hz, 1H), 6.75 (t, J = 8.5 Hz, 1H), 6.39 (s, 2H), 3.81 (s, 3H), 3.76 (s, 3H), 3.74 (s, 6H), 3.51 (d, J = 6.56 Hz, 1H), 3.49 (d, J = 6.56 Hz, 1H). ^{13}C NMR (150 MHz, $CDCl_3$) δ 152.65, 151.06, 146.36, 146.29, 136.67, 132.06, 129.81, 129.77, 123.58, 123.56, 115.86, 115.74, 112.73, 104.73, 60.80, 56.21, 55.96, 39.90, 39.17. ESI-HRMS (m/z): calcd for $C_{18}H_{20}FNO_4$ ($M + H^+$), 334.1449; found, 334.1445.

4.5.2. 2-(3-fluoro-4-methoxyphenyl)-1-methyl-3-(3,4,5-trimethoxyphenyl)aziridine (**7b**)

7a (25 mg, 0.075 mmol) and MeI (2 mL) were charged into a round-bottom bottle. The mixture was allowed to be stirred at room temperature for 3 h, which was then concentrated under reduced pressure. The resulting residue was purified by silica gel column chromatography (elute with ethyl acetate/hexane = 2:1, v/v) to give **7b** as white solid (21 mg, yield 81%), Mp 110.6–112.8 °C. ^{1}H NMR (400 MHz, $CDCl_3$) δ 6.97 (d, J = 12.4 Hz, 1H), 6.87 (d, J = 8.4 Hz, 1H), 6.75 (t, J = 8.5 Hz, 1H), 6.35 (s, 2H), 3.81 (s, 3H), 3.75 (s, 3H), 3.73 (s, 6H), 2.76 (d, J = 6.48 Hz, 1H), 2.72 (d, J = 6.48 Hz, 1H), 2.68 (s, 3H). ^{13}C NMR (150 MHz, $CDCl_3$) δ 152.67, 151.08, 146.30, 146.22, 136.60, 131.97, 129.68, 129.64, 123.47, 115.82, 115.69, 112.79, 104.63, 60.80, 56.25, 55.95, 50.54, 49.70, 47.77.ESI-HRMS (m/z): calcd for $C_{19}H_{22}FNO_4Na$ ($M + Na^+$), 370.1403; found, 370.1425.

4.6. Procedure for the synthesis of chiral aziridine derivatives

4.6.1. (2R,3S)-2-(3-fluoro-4-methoxyphenyl)-3-(3,4,5-trimethoxyphenyl)aziridine ((+)-**7a**)

A mixture of (+)-**6h** (115 mg, 0.345 mmol) and sodium borohydride (50 mg, 1.39 mmol) in tetrahydrofuran (5 mL) and methanol (5 mL) was stirred at room temperature for 2 h. The solvent was removed under reduced pressure and the residue was directly purified by flash column chromatography (elute with ethyl acetate/hexane = 2:1, v/v) to give the title compound (+)-**7a** as yellow solid (105 mg, yield 91%), Mp 117.4–120.3 °C. ^{1}H NMR (400 MHz, $CDCl_3$) δ 6.99 (dd, J = 12.4, 1.8 Hz, 1H), 6.91 (d, J = 8.4 Hz, 1H), 6.75 (t, J = 8.5 Hz, 1H), 6.39 (s, 2H), 3.81 (s, 3H), 3.76 (s, 3H), 3.74 (s, 6H), 3.50 (q, J = 6.5 Hz, 2H). ^{13}C NMR (150 MHz, $CDCl_3$) δ 152.65, 151.06, 146.36, 146.29, 136.67, 132.06, 129.81, 129.77, 123.58, 123.56, 115.86, 115.74, 112.73, 104.73, 60.80, 56.21, 55.96, 39.90, 39.17. ESI-HRMS (m/z): calcd for $C_{18}H_{20}FNO_4$ ($M + H^+$), 334.1449; found, 334.1445.

4.6.2. (2R,3S)-2-(3-fluoro-4-methoxyphenyl)-1-((4-nitrophenyl) sulfonyl)-3-(3,4,5-trimethoxyphenyl)aziridine (**8**)

A mixture of (+)-**7a** (20 mg, 0.06 mmol), 4-nitrobenzenesulphonyl chloride (20 mg, 0.09 mmol), triethylamine (17 μL, 0.12 mmol) and 4-dimethylaminopyridine (1 mg, 0.01 mmol) in dichloromethane (5 mL) was stirred at room temperature for 1 h. The solvent was removed under reduced pressure and the residue was directly purified by flash column chromatography (elute with ethyl acetate/petroleum ether = 1:5, v/v) to give the title compound **8** as yellow solid (27 mg, yield 87%), Mp 133.1–134.2 °C. ^{1}H NMR (400 MHz, $CDCl_3$) δ 8.42 (d, J = 8.9 Hz, 2H), 8.27 (d, J = 9.0 Hz, 2H), 6.85–6.72 (m, 3H), 6.22 (s, 2H), 4.28–4.20 (m, 2H), 3.80 (s, 3H), 3.75 (s, 3H), 3.65 (s, 6H).^{13}C NMR (150 MHz, $CDCl_3$) δ153.06, 152.72, 151.08, 150.83, 147.70, 147.63, 143.69, 138.03, 129.29, 126.38, 124.52, 124.11, 124.07, 123.70, 115.59, 115.46, 113.08, 104.84, 60.82, 56.19, 56.02, 48.34, 47.44. ESI-HRMS (m/z): calcd for $C_{24}H_{23}FN_2O_8S$ ($M + Na^+$), 541.1051; found, 541.1050.

Single crystals of **8** suitable for X-ray crystallographic analysis were obtained by slow evaporation of a solution of **8** in petroleum ether/dichloromethane (Table 4).

CIF file of **8** can be obtained from the Cambridge Crystallographic Data Centre using deposition number CCDC2036521. Copies of the data can be obtained, free of charge, on application to the CCDC, 12 Union Road, Cambridge CB2 1EZ, UK [fax: +44(1223) 336033; e-mail: deposit@ccdc.cam.ac.uk].

4.7. In vitro cell growth inhibition assay

Human ovarian carcinoma (A2780), human colonic adenoma (HCT-116), human lung adenocarcinoma (A549), human cervical carcinoma (HeLa) and immortalized T-lymphocyte (Jurkat) were

Table 4
Crystal data for **8**.

Temperature	170.01 K
Wavelength	1.34139 Å
Crystal system	Monoclinic
Space group	C 1 2 1
Unit cell dimensions	a = 21.7846(5) Åa = 90°
b = 7.7471(2) Å	b = 123.5070(10)°.
c = 18.7739(4) Å	g = 90°.
Volume	2641.89(11) Å^3
Z	4
Density (calculated)	1.454 Mg/m^3
Absorption coefficient	1.969 mm^{-1}
F(000)	1196
Crystal size	0.12 × 0.06 × 0.05 mm^3
Theta range for data collection	3.532–54.971°.
Index ranges	−26 ≤ h<=23, −6 ≤ k<=9, −22 ≤ l<=22
Reflections collected	11981
Independent reflections	4427 [R(int) = 0.0454]
Completeness to theta = 53.594°	99.7%
Absorption correction	Semi-empirical from equivalents
Max. and min. transmission	0.7508 and 0.5628
Refinement method	Full-matrix least-squares on F^2
Data/restraints/parameters	4427/24/365
Goodness-of-fit on F^2	1.043
Final R indices [I > 2sigma(I)]	R1 = 0.0461, w*R*2 = 0.0975
R indices (all data)	R1 = 0.0572, w*R*2 = 0.1050
Absolute structure parameter	0009(15)
Extinction coefficient	n/a
Largest diff. peak and hole	0.604 and −0.417 e.Å^{-3}

cultivated in Dulbecco's modified Eagle medium (DMEM) containing 100 units/mL penicillin G, 100 μg/mL streptomycin and 10% (v/v) fetal bovine serum in 37 °C and 5% carbon dioxide atmosphere.

The anti-proliferative of compounds were evaluated by employing MTT assay. Cells were seeded in 96-well plates for 24 h. Then cells were treated with different concentrations of compounds for 48 h. 20 μL MTT solution (5 mg/mL) was added to each well, followed by incubating for another 4 h at 37 °C. Then, the suspension was discarded and DMSO (150 μL) was added to each well. The plates were read by microplate reader (Biotech ELx800) at the wavelength of 570 nm and half maximal inhibitory concentration (IC_{50}) was counted using software GraphPad Prism (version 6.0).

4.8. Colony formation assay

HeLa cells were seeded into a six-well plate. After being cultured at 37 °C for 24 h, the cells were treated with gradient concentrations of **6h** or DMSO (negative control) for 48 h, followed by replacing the agents by fresh medium and incubation at 37 °C for additional 7–10 days. Then the cells were dyed with gentian violet staining solution for 30 min and washed twice with fresh phosphate buffer saline. The stained colonies were counted and compared with the control cells.

4.9. In vitro tubulin polymerization assay

Pig brain microtubule protein was commercially available. Compound **6h** with a range of concentrations, colchicine (positive control) or DMSO (negative control) were treated with a solution of tubulin protein in G-PEM buffer (100 mM PIPES, 10 mM $MgCl_2$, 1 mM EGTA, 1 mM GTP and 3.4 M glycerol). Then the mixtures were transferred to 37 °C and detected light scattering at 340 nm using a SPECTRA MAX 190 (Molecular Device) spectrophotometer. And the plateau absorbance values were used for calculations.

4.10. Cell cycle analysis

HeLa cells were seeded into a six-well plate and being cultured at 37 °C for 24 h. After treatment with gradient concentrations of **6h** or DMSO (negative control) for 24 h, cells were collected, centrifuged and fixed with 75% ethanol at −20 °C overnight. Fixed cells were treated with RNase A solution and stained with a propidium iodide containing PBS solution at room temperature in dark conditions. Cell cycle analysis was determined with Multicycle AV (for Windows, version 320) software.

4.11. Cell apoptosis analysis

HeLa cells growth was seeded into each well of six-well plate. After incubation overnight, cells were treated with gradient concentrations of **6h** or DMSO (negative control) for 48 h. Then the cells were collected, centrifuged and resuspended in staining solution (containing Annexin V-FITC and propidium iodide in Binding Buffer) in the dark place for 15 min. Samples were analyzed on flow cytometer (Cytomics FC 500 MPL, Beckman Coulter) analysis.

4.12. Western blot analysis

After treatment with gradient concentrations of **6h** or DMSO (negative control), HeLa cells were collected, washed twice with phosphate buffer saline and lysed with cell lysis buffer. After centrifugation for 30 min at 4 °C, supernatant was obtained. Protein concentrations were determined by BCA protein assay kit. Then protein samples were separated by SDS-PAGE electrophoresis and transferred onto polyvinylidene fluoride (PVDF) membranes. After being blocked with 5% BSA in TBST, membranes were interacted with diluted primary antibodies at 4 °C overnight and incubated with horseradish peroxidase (HRP) labeled secondary antibodies at room temperature. Finally, protein was detected by chemiluminescent reagent.

4.13. Immunofluorescent analysis

HeLa cells were cultured with DMSO (negative control) or the tested compound with different concentrations overnight, HeLa cells were fixed by methanol, permeabilized with 0.1% Triton X-100 and incubated in 3% BSA for 1 h. Then cells were incubated with α-tubulin monoclonal antibody overnight at 4 °C and stained with Alexa 488 labeled secondary antibody dilution. Then the nucleus of cells were stained with DAPI for 10 min at room temperature. Images were collected by a Leica SP5 co-focal fluorescence microscope.

4.14. Tube formation assay

Matrigel was added into a 96-well plate and incubated at 37 °C for 2 h to emerge its polymerization morphology, and human umbilical vein endothelial cells (HUVECs) suspended in DMEM were seeded afterwards. They were then treated with The tested compound with different concentrations or DMSO (negative control). After incubation for 12 h at 37 °C, capillary-like tube formed, and cells were photographed with a CCD Sensicam camera attached to an inverted microscope.

4.15. Comet assay

The following processes should be operated in the darkness to avoid additional DNA damage. Jurkat cells were seeded into a six-well plate and then exposed to various concentrations of tested compounds, MMC (positive control), or DMSO (negative control)

and incubated at 37 °C for 48 h, followed by combination with molten LM Agarose and were immediately pipette onto Comet Slide, which were immersed in Lysis buffer successively and incubated for 2 h at 4 °C. Slides were dipped into alkaline unwinding solution (1 mM EDTA, 200 mM NaOH) for 30 min, followed by electrophoresis solution (1 mM EDTA, 200 mM NaOH) at 25 V for 15 min, and washed twice in water. The slides were stained with ethidium bromide (EB) and washed twice with water. The results were visualized by microscopy (OLYMPOS BX51). Under these conditions the formation of "comet tail" is indicative of DBSs, SSDs, and/or active excision repair of DNA cross-links.

4.16. Xenografts tumor growth assay in nude mice

We purchased 6 weeks old female Balb/C nude mice from Shanghai Slac Laboratory Animal Co. Ltd. (Shanghai, China), and implanted A2780 cells suspended in PBS in the right flank of mice. When tumor volumes reached 100 mm^3, mice were treated with compound **6h** (25, 50 mg/kg), PTX (10 mg/kg) or vehicle (containing 10% castor oil and 10% DMSO in PBS) every two days. Tumor volumes and body weights were gauged when administrated with a digital caliper each time (calculated volume (mm^3) = (π/6) × length × width × width). The mice were sacrificed and the tumors were isolated and weighed subsequently when the average tumor volume reached 2000 mm^3. The animal experimental protocols were approved by the Animal Ethics Committee of School of Pharmacy, Fudan University.

4.17. Enantiomeric separation

The separation was performed on the Themo Fisher Ultimate 3000 HPLC equipped with Daicel Chiralpak IC. The mobile phase was n-hexane/i-PrOH (80/20, v/v) with flow rate of 1.0 mL/min. The UV response was detected under 230 nm at 25 °C.

The specific rotation data were recorded at 25 °C on a Rudolph Autopol IV polarimeter with 1.0 mg/mL of each enantiomer in $CHCl_3$.

4.18. Preliminary stability study

The solution of **6h** (5 mg/mL in methanol, 20 μL) was mixed with phosphate buffers (480 μL, pH 7.4). The resulted solutions were filtered by 0.22 μm microfiltration membrane. The filtrate were analyzed by HPLC (Poroshell 120 EC-C18 3.0 × 50 mm, 2.7 μm; mobile phase methanol/H_2O, 60:40, 1 mL/min) after 4 h, 8 h, 12 h, 24 h and 48 h under pH 7.4 condition, respectively. 95.77% of compound **6h** was recovered at pH 7.4 media after 48 h.

Author contributions

The manuscript was written through contributions of all authors./All authors have given approval to the final version of the manuscript.

Notes

The authors declare no competing financial interest.

Declaration of competing interest

The authors declare that they have no known competing financial interests or personal relationships that could have appeared to influence the work reported in this paper.

Acknowledgements

This work was supported by grants from the National Natural Science Foundation of China (21877015) and Science and Technology Commission of Shanghai Municipality (20S11902500).

Appendix A. Supplementary data

Supplementary data related to this article can be found at https://doi.org/10.1016/j.ejmech.2021.113256.

References

[1] A. Jordan, J.A. Hadfield, N.J. Lawrence, A.T. Mcgown, Tubulin as a target for anticancer drugs: agents which interact with the mitotic spindle, Med. Res. Rev. 18 (1998) 259–296.
[2] R. Heald, E. Nogales, Microtubule dynamics, J. Cell Sci. 115 (2002) 3–4.
[3] J.R. McIntosh, E. Grishchuk, R.R. West, Chromosome-microtubule interactions during mitosis, Annu. Rev. Cell Dev. Biol. 18 (2002) 193–219.
[4] M. Kavallaris, Microtubules and resistance to tubulin-binding agents, Nat. Rev. Canc. 10 (2010) 194–204.
[5] G.G. Dark, S.A. Hill, V.E. Prise, G.M. Tozer, G.R. Pettit, D. J Chaplin, Combretastatin A-4, an agent that displays potent and selective toxicity toward tumor vasculature, Canc. Res. 57 (1997) 1829–1834.
[6] R. Mikstacka, T. Stefanski, J. Rozanski, Tubulin-interactive stilbene derivatives as anticancer agents, Cell. Mol. Biol. Lett. 18 (2013) 368–397.
[7] G.C. Tron, T. Pirali, G. Sorba, F. Pagliai, S. Busacca, A.A. Genazzani, Medicinal chemistry of combretastatin A4: present and future directions, J. Med. Chem. 49 (2006) 3033–3044.
[8] L. Li, S. Jiang, X. Li, Y. Liu, J. Su, J. Chen, Recent advances in trimethoxyphenyl (TMP) based tubulin inhibitors targeting the colchicine binding site, Eur. J. Med. Chem. 151 (2018) 482–494.
[9] Y. Lu, J. Chen, M. Xiao, W. Li, D.D. Miller, Anoverview of tubulin inhibitors that interact with the colchicine binding site, Pharm. Res. (N. Y.) 29 (2012) 2943–2971.
[10] N.M. O'Boyle, J.K. Pollock, M. Carr, A.J.S. Knox, S.M. Nathwani, S. Wang, L. Caboni, D.M. Zisterer, M.J. Meegan, β-Lactam estrogen receptor antagonists and a dual-targeting estrogen receptor/tubulin ligand, J. Med. Chem. 57 (2014) 9370–9382.
[11] P. Zhou, Y. Liu, L. Zhou, K. Zhu, K. Feng, H. Zhang, Y. Liang, H. Jiang, C. Luo, M. Liu, Y. Wang, Potent antitumor activities and structure basis of the chiral β-lactam bridged analogue of combretastatin A-4 binding to tubulin, J. Med. Chem. 59 (2016) 10329–10334.
[12] M. Zhang, Y.R. Liang, H. Li, M. Liu, Y. Wang, Design, synthesis, and biological evaluation of hydantoin bridged analogues of combretastatin A-4 as potential anticancer agents, Bioorg. Med. Chem. 25 (2017) 6623–6634.
[13] R. Romagnoli, P.G. Baraldi, A. Brancale, A. Ricci, E. Hamel, R. Bortolozzi, G. Basso, G. Viola, Convergent synthesis and biological evaluation of 2-amino-4-(3',4',5'-trimethoxyphenyl)-5-aryl thiazoles as microtubule targeting agents, J. Med. Chem. 54 (2011) 5144–5153.
[14] S. Theeramunkong, A. Caldarelli, A. Massarotti, S. Aprile, D. Caprioglio, R. Zaninetti, A. Teruggi, T. Pirali, G. Grosa, G.G. Tron, Regioselectivesuzuki coupling of dihaloheteroaromatic compounds as a rapid strategy to synthesize potent rigid combretastatin analogues, J. Med. Chem. 54 (2011) 4977–4986.
[15] F. Gao, Y. Liang, P. Zhou, J. Cheng, K. Ding, Y. Wang, Design, synthesis, antitumor activities and biological studies of novel diaryl substituted fused heterocycles as dual ligands targeting tubulin and katanin, Eur. J. Med. Chem. 178 (2019) 177–194.
[16] Y.N. Liu, J.J. Wang, Y.T. Ji, G.D. Zhao, L.Q. Tang, C.M. Zhang, X.L. Guo, Z.P. Liu, Design, synthesis, and biological evaluation of 1-methyl-1,4-dihydroindeno [1,2-c]pyrazole analogues as potential anticancer agents targeting tubulin colchicine binding site, J. Med. Chem. 59 (2016) 5341–5355.
[17] A. Stornetta, M. Zimmermann, G.D. Cimino, P.T. Henderson, S.J. Sturla, DNA adducts from anticancer drugs as candidate predictive markers for precision medicine, Chem. Res. Toxicol. 30 (2017) 388–409.
[18] M.D. Urbaniak, J.P. Bingham, J.A. Hartley, D.N. Woolfson, S. Caddick, Design and synthesis of a nitrogen mustard derivative stabilized by apo-neocarzinostatin, J. Med. Chem. 47 (2004) 4710–4715.
[19] A.A. Nazarov, S.M. Meier, O. Zava, Y.N. Nosova, E.R. Milaeva, C.G. Hartinger, P.J. Dyson, Protein ruthenation and DNA alkylation: chlorambucil-functionalized RAPTA complexes and their anticancer activity, Dalton Trans. 44 (2015) 3614–3623.
[20] B.S. Iyengar, R.T. Dorr, D.S. Alberts, E.M. Hersh, S.E. Salmon, W.A. Remers, Novel antitumor 2-cyanoaziridine-1-carboxamides, J. Med. Chem. 42 (1992) 510–514.
[21] E. Wall, J.H. Beijnen, S. Rodenhuis, High-dose chemotherapy regimens for solid tumors, Canc. Treat Rev. 21 (1995) 105–132.
[22] W.T. Bradner, Mitomycin C: a clinical update, Canc. Treat Rev. 27 (2001) 35–50.
[23] S.S. Pan, P.A. Andrews, C.J. Glover, N.R. Bachur, Reductive activation of mitomycin C and mitomycin C metabolites catalyzed by NADPH-cytochrome P-

450 reductase and xanthine oxidase, J. Biol. Chem. 259 (1984) 959–966.
[24] V.J. Spanswick, J. Cummings, J.F. Smyth, Enzymology of mitomycin C metabolic activation in tumour tissue: characterization of a novel mitochondrial reductase, Biochem. Pharmacol. 51 (1998) 405.
[25] M. Sastry, R. Fiala, R. Lipman, M. Tomasz, D.J. Patel, Solution structure of the monoalkylated mitomycin C-DNA complex, J. Mol. Biol. 247 (1995) 338.
[26] C.M. Mallory, R.P. Carfi, S.P. Moon, K.A. Cornell, D.L. Warner, Modification of cellular DNA by synthetic aziridinomitosenes, Bioorg. Med. Chem. 23 (2015) 7378–7385.
[27] X. Qin, L. Fang, F. Chen, S. Gou, Conjugation of platinum (IV) complexes with chlorambucil to overcome cisplatin resistance via a "joint action" mode toward DNA, Eur. J. Med. Chem. 137 (2017) 167–175.
[28] S.M. Musser, S.S. Pan, M.J. Egorin, D. J Kyle, P. S Callery, Alkylation of DNA with aziridine produced during the hydrolysis of N,N',N''-triethylenethiophosphoramide, Chem. Res. Toxicol. 5 (1992) 95–99.
[29] H. Kostrhunova, J. Zajac, V. Novohradsky, J. Kasparkova, J. Malina, J.R. Aldrich-Wright, E. Petruzzella, R. Sirota, D. Gibson, V. Brabec, A subset of new platinum antitumor agents kills cells by a multimodal mechanism of action also involving changes in the organization of the microtubule cytoskeleton, J. Med. Chem. 62 (2019) 5176–5190.
[30] R. Schobert, B. Biersack, A. Dietrich, S. Knauer, M. Zoldakova, A. Fruehauf, T. Mueller, Pt (II) complexes of a combretastatin A-4 analogous chalcone: effects of conjugation on cytotoxicity, tumor specificity, and long-term tumor growth suppression, J. Med. Chem. 52 (2009) 241–246.
[31] P. Diana, A. Martorana, P. Barraja, A. Montalbano, G. Dattolo, G. Cirrincione, F.D. Acqua, A. Salvador, D. Vedaldi, G. Basso, G. Viola, Isoindolo[2,1-a] quinoxaline derivatives, novel potent antitumor agents with dual inhibition of tubulin polymerization and topoisomerase I, J. Med. Chem. 51 (2008) 2387–2399.
[32] L. Li, X. Huang, R. Huang, S. Gou, Z. Wang, H. Wang, Pt(IV) prodrugs containing microtubule inhibitors displayed potent antitumor activity and ability to overcome cisplatin resistance, Eur. J. Med. Chem. 156 (2018) 666–679.
[33] X. Huang, R. Huang, Z. Wang, L. Li, S. Gou, Z. Liao, H. Wang, Pt(IV) complexes conjugating with chalcone analogue as inhibitors of microtubule polymerization exhibited selective inhibition in human cancer cells, Eur. J. Med. Chem. 146 (2018) 435–450.
[34] X. Huang, R. Huang, S. Gou, Z. Wang, Z. Liao, H. Wang, Combretastatin A-4 analogue: a dual-targeting and tubulin inhibitor containing antitumor Pt(IV) moiety with a unique mode of action, Bioconjugate Chem. 27 (2016) 2132–2148.
[35] Y. Zhang, M. Zhai, Z. Chen, X. Han, F. Yu, Z. Li, X. Xie, C. Han, L. Yu, Y. Yang, X. Mei, Dual-modified liposome codelivery of doxorubicin and vincristine improve targeting and therapeutic efficacy of glioma, Drug Deliv. 24 (2017) 1045–1055.
[36] S. Yu, L. Qi, K. Hu, J. Gong, T. Cheng, Q. Wang, J. Chen, H. Wu, The development of a palladium-catalyzed tandem addition/cyclization for the construction of indole skeletons, J. Org. Chem. 82 (2017) 3631–3638.
[37] M.N. Zhao, W. Zhang, X.C. Wang, Y. Zhang, D. Yang, Z. Guan, Modular 2,3-diaryl-2*H*-azirine synthesis from ketoxime acetates via Cs_2CO_3-mediated cyclization, Org. Biomol. Chem. 16 (2018) 4333–4337.
[38] H. Hu, Y. Liu, L. Lin, Y. Zhang, X. Liu, X. Feng, Kinetic resolution of 2*H*-azirines by asymmetric imine amidation, Angew. Chem. Int. Ed. 55 (2016) 10098–10101.
[39] G. Speit, A. Hartmann, The comet assay: a sensitive genotoxicity test for the detection of DNA damage and repair, Methods Mol. Biol. 314 (2006) 79–90.
[40] Q. Cui, J. Yu, J. Wu, S. Tashiro, S. Onodera, M. Minami, T. Ikejima, P53-mediated cell cycle arrest and apoptosis through a caspase-3-independent, but caspase-9-dependent pathway in oridonin-treated MCF-7 human breast cancer cells, Acta Pharmacol. Sin. 28 (2007) 1057–1066.